Absence of MHC class II on cDCs results in microbial-dependent intestinal inflammation

Jakob Loschko,[1] Heidi A. Schreiber,[1] Gereon J. Rieke,[1,5] Daria Esterházy,[2] Matthew M. Meredith,[1] Virginia A. Pedicord,[2] Kai-Hui Yao,[1] Silvia Caballero,[4] Eric G. Pamer,[4] Daniel Mucida,[2] and Michel C. Nussenzweig[1,3]

[1]Laboratory of Molecular Immunology, [2]Laboratory of Mucosal Immunology, and [3]Howard Hughes Medical Institute, The Rockefeller University, New York, NY, 10065
[4]Immunology Program, Sloan Kettering Institute Infectious Diseases Service Clinical Microbiology Laboratory, Memorial Sloan Kettering Cancer Center, New York, NY, 10065
[5]Rheinische Friedrich-Wilhelms University Bonn, 53113 Bonn, Germany

Conventional dendritic cells (cDCs) play an essential role in host immunity by initiating adaptive T cell responses and by serving as innate immune sensors. Although both innate and adaptive functions of cDCs are well documented, their relative importance in maintaining immune homeostasis is poorly understood. To examine the significance of cDC-initiated adaptive immunity in maintaining homeostasis, independent of their innate activities, we generated a cDC-specific Cre mouse and crossed it to a floxed MHC class II (MHCII) mouse. Absence of MHCII on cDCs resulted in chronic intestinal inflammation that was alleviated by antibiotic treatment and entirely averted under germ-free conditions. Uncoupling innate and adaptive functions of cDCs revealed that innate immune functions of cDCs are insufficient to maintain homeostasis and antigen presentation by cDCs is essential for a mutualistic relationship between the host and intestinal bacteria.

Conventional DCs (cDCs) are specialized immune cells that link the innate and adaptive immune system. Innate features of cDCs allow them to recognize and respond to pathogens by producing essential cytokines such as IL-6, IL-12, IL-23, and TNF. These cytokines contribute to the activation of other immune cells, including T and B cells and cells of the innate immune system. For example, in the intestine, cDCs sense bacteria and produce IL-23, which induces type III innate lymphoid cells (ILC3s) to produce IL-22, which in turn stimulates production of antimicrobial peptides (AMPs; Sonnenberg et al., 2011; Kinnebrew et al., 2012; Satpathy et al., 2013; Bernink et al., 2015). In addition to their innate functions, cDCs initiate adaptive immune responses by ingesting, processing, and presenting antigens to T cells (Nussenzweig et al., 1980; Steinman et al., 2003). In the intestine, cDCs are responsible for transport of antigen to the draining mesenteric LNs (mLNs). Under physiological conditions, the capacity of cDCs to migrate from tissue to draining LNs distinguishes them from more sessile macrophages (Schreiber et al., 2013). The importance of cDCs in adaptive immune function is exemplified by the fact that cDC depletion during viral and bacterial infection results in impaired T cell immunity and increased susceptibility to infection (Jung et al., 2002; Kassim et al., 2006; Hildner et al., 2008; Satpathy et al., 2013; Schreiber et al., 2013).

In mice, expression of *Itgax* (CD11c) is a hallmark of the DC lineage, and its expression has been used to label ($CD11c^{YFP}$), deplete ($CD11c^{DTR}$), and conditionally target ($CD11c^{Cre}$) cDCs (Jung et al., 2002; Lindquist et al., 2004; Caton et al., 2007; Stranges et al., 2007). However, CD11c is also expressed by plasmacytoid DCs (pDCs), activated monocytes, macrophages, and some NK cells, and therefore CD11c-based labeling and targeting strategies are not entirely cDC specific (Serbina et al., 2003; Hohl et al., 2009; Meredith et al., 2012; Schreiber et al., 2013). Higher levels of specificity can be achieved by deletion of genes that regulate the development of specific subsets of cDCs, such as *Batf3*, *Irf4*, and *Notch2*; however, these methods have yet to be applied to dissect the relative contributions of the innate and adaptive functions of cDCs to immune homeostasis (Caton et al., 2007; Hildner et al., 2008; Persson et al., 2013; Schlitzer et al., 2013).

To investigate the adaptive functions of cDCs independent of innate activities, we produced a cDC-restricted Cre mouse wherein Cre expression is directed by the *Zbtb46* gene (zDC^{Cre}) and used it to delete MHCII in cDCs in vivo. These mice exhibited profound intestinal inflammation that was directly related to the presence of intestinal bacteria, as antibiotic-treated or germ-free mice lacking MHCII on cDCs showed no signs of intestinal inflammation. Colonization of germ-free

Correspondence to Michel C. Nussenzweig: nussen@rockefeller.edu

Abbreviations used: AMP, antimicrobial peptides; cDC, conventional DC; FISH, fluorescence in situ hybridization; ILC3, type III innate lymphoid cell; mLN, mesenteric LN; pDC, plasmacytoid DC; pIC, polyinosinic:polycytidylic acid; PP, Peyer's patches; qPCR, quantitative PCR; RPM, red pulp macrophage; rRNA, ribosomal RNA; SPF, specific pathogen–free.

The Rockefeller University Press $30.00
J. Exp. Med. 2016 Vol. 213 No. 4 517–534
www.jem.org/cgi/doi/10.1084/jem.20160062

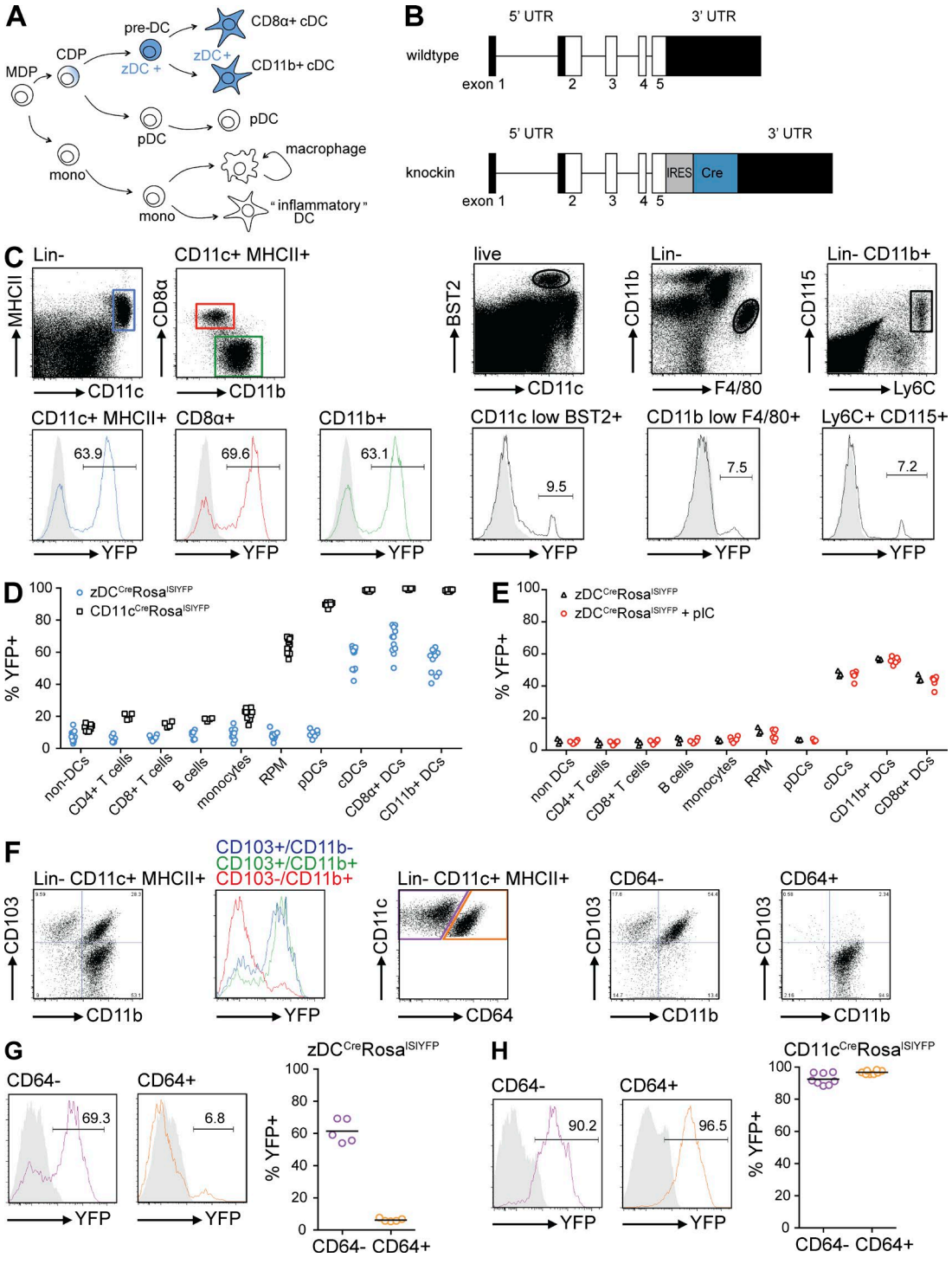

Figure 1. **zDC^{Cre} mouse.** (A) Diagram shows development of mononuclear phagocytes, with zDC-expressing cells in blue. (B) Schematic diagram of the *Zbtb46* locus. 5′ and 3′ UTRs are shown in black, and coding regions are shown in white. (C) Flow cytometric analysis of splenic cDCs (Lin$^-$CD11c^{high}MHCII$^+$), pDCs (CD11c^{low}BST2$^+$), RPMs (Lin$^-$CD11b$^-$F4/80$^+$), and monocytes (Lin$^-$CD11b$^+$Ly6C$^+$CD115$^+$). Histograms show percentage of cells expressing YFP in zDC^{Cre}Rosa^{lSlYFP} mice (open histograms) or Rosa^{lSlYFP} control mice (filled gray histograms). (D) Graph depicts percentage of various immune cell populations in the spleen expressing YFP in zDC^{Cre}Rosa^{lSlYFP} mice (blue symbols) and CD11c^{Cre}Rosa^{lSlYFP} mice (black symbols). Each data point represents one individual mouse (n = 4–13). (E) Splenocytes were isolated 16 h after i.p. administration of 10 µg pIC. Graph depicts percentage of various immune cell populations expressing YFP in zDC^{Cre}Rosa^{lSlYFP} mice (black symbols) and zDC^{Cre}Rosa^{lSlYFP} mice that received pIC (red symbols). Each data point represents one individual mouse (n = 3–6). (F) Flow cytometric analysis of small intestine lamina propria mononuclear phagocytes (Lin$^-$CD11c$^+$MHCII$^+$). Histogram shows YFP expression of DC subsets

mice allowed us to monitor adaptive immune responses against intestinal bacteria and revealed that mice lacking MHCII on cDCs have a defect in inducing proper adaptive immune responses against commensals. Collectively, our studies reveal the importance of the adaptive function of cDCs in maintaining intestinal homeostasis.

RESULTS

Generation of zDC^{Cre} mouse

Zbtb46 (zDC) is expressed in pre-DCs and their progeny, but not in monocytes, macrophages, and other myeloid cells (Fig. 1 A; Meredith et al., 2012; Satpathy et al., 2012). To express Cre recombinase in cells that actively transcribe zDC, we inserted Cre into the 3′ UTR of z*DC* (Fig. 1 B; Meredith et al., 2012). Cell type–specific expression of Cre was confirmed by crossing zDC^{Cre} to Rosa26^{lslYFP} mice (zDC^{Cre}Rosa^{lslYFP}), wherein Cre-mediated excision of a transcriptional Stop element results in YFP expression. The majority of cDCs (Lin$^-$CD11c^{high}MHCII$^+$) in the spleen of zDC^{Cre}Rosa^{lslYFP} mice were YFP$^+$. In contrast, B and T lymphocytes, pDCs (CD11c^{low}BST2$^+$), red pulp macrophages (RPMs; Lin$^-$CD11b^{low}F4/80$^+$), and monocytes (Lin$^-$CD11b$^+$Ly6C$^+$CD115$^+$) expressed little or no YFP (Fig. 1, C and D). In contrast, in CD11c^{Cre}Rosa^{lslYFP} mice, cDCs, as well as the majority of macrophages, and pDCs were labeled in the spleen (Fig. 1 D). Similar results were also obtained after administration of polyinosinic:polycytidylic acid (pIC; Fig. 1 E) and with zDC^{Cre+}IRF4$^{wt/fl}$ mice that express GFP upon Cre-mediated IRF4 excision (Klein et al., 2006; Fig. S1).

In the intestine, the phenotype of monocytes and cDCs is altered (Caballero and Pamer, 2015). For example, small intestine lamina propria CD11c$^+$MHCII$^+$ cells represent a mixture of cDCs and monocytes that can be further subdivided based on expression of CD103, CD11b, and CD64 (Fig. 1 F; Bogunovic et al., 2009; Tamoutounour et al., 2012; Schreiber et al., 2013). Whereas all of these cell types are labeled in CD11c^{Cre}Rosa^{lslYFP} mice, only pre-DC–derived CD64$^-$ cells were YFP$^+$ in zDC^{Cre}Rosa^{lslYFP} indicator mice (Fig. 1, G and H). We did not observe a difference in YFP expression in CD103$^+$/CD11b$^-$ and CD103$^+$/CD11b$^+$ CD64$^-$ cells in zDC^{Cre}Rosa^{lslYFP} mice (Fig. 1 F). We conclude that zDC^{Cre} mice are suitable for cDC-specific conditional gene deletion.

zDCΔMHCII mice exhibit preserved innate functions but impaired adaptive functions

In addition to antigen processing and presentation, cDCs are essential innate sensors of pathogens and other stimuli. To distinguish between innate and adaptive functions of cDCs, we produced a cDC-specific MHCII knockout by crossing zDC^{Cre} with MHCII$^{fl/fl}$ mice (zDCΔMHCII; Hashimoto et al., 2002). As expected, zDCΔMHCII mice expressed MHCII on the surface of pDCs, but not on cDCs (Fig. 2 A). Absence of MHCII expression by cDCs did not change the frequency of cDCs among splenocytes (Fig. 2 B), nor did it alter the ratio of CD8α$^+$ and CD11b$^+$ cDCs (Fig. 2 C). The same was true for the mLNs (Fig. 2, D and E). Moreover, the levels of circulating Flt3L in the serum, which are increased upon cDC depletion (Birnberg et al., 2008; Meredith et al., 2012), were normal in zDCΔMHCII mice (Fig. 2 F).

To determine whether adaptive responses are altered by cDC-specific MHCII deletion, we transferred OVA-specific CD4$^+$ T cells (OT-II cells) to control and zDCΔMHCII mice and compared their responses to immunization with OVA. OT-II cells responded by proliferating and up-regulating CD44 expression in control but not in zDCΔMHCII mice (Fig. 2, G and H). In contrast, proliferation and activation of CD8$^+$ OT-I T cells in response to immunization with OVA was not altered in zDCΔMHCII mice (Fig. 2, G and H). Thus, deletion of MHCII on the surface of cDCs is sufficient to impair priming of naive CD4$^+$ T cells.

To confirm that the innate responses of cDCs are intact in zDCΔMHCII mice, we purified cDCs from the spleen, stimulated them with CpG 1668, LPS, or pIC, and measured expression of co-stimulatory molecules (CD80 and CD86) and production of cytokines (IL-6 and TNF). We found no differences between control and zDCΔMHCII cDCs, indicating that their responses to innate stimuli are intact (Fig. 2 I–M). Thus, zDCΔMHCII cDCs show intact responses to innate stimuli, but are unable to initiate MHCII-restricted adaptive immune responses.

Intestinal inflammation develops in mice lacking MHCII on cDCs

Although zDCΔMHCII mice were born at the expected Mendelian ratio, they showed significantly reduced weight gain (Fig. 3 A) and developed rectal prolapse starting at 6 wk of age (Fig. 3 B). In addition, the mutant mice concomitantly developed splenomegaly and showed increased circulating levels of the acute phase–reactant Csf3 and neutrophilia, which are indicative of a systemic process (Fig. 3, C–E). The levels of Csf1 and Csf2 remained within normal limits (unpublished data).

To quantitate intestinal inflammation, we measured Lipocalin-2, a sensitive biomarker for intestinal inflammation, in the feces of control and zDCΔMHCII mice (Chassaing et al., 2012). zDCΔMHCII mice showed a 100-fold increase in Lipocalin-2 compared with controls (Fig. 3 F). Consistent with this observation, histopathological analysis revealed inflammation that was primarily restricted to the large intestine,

in zDC^{Cre}Rosa^{lslYFP} mice. (G and H) Histograms show expression of YFP in zDC^{Cre}Rosa^{lslYFP} mice (G, open histograms) and CD11c^{Cre}Rosa^{lslYFP} mice (H, open histograms) or Rosa^{lslYFP} control mice (filled gray histograms). Graphs depict percentage of CD64$^-$ and CD64$^+$ DCs expressing YFP in zDC^{Cre}Rosa^{lslYFP} (G) and CD11c^{Cre}Rosa^{lslYFP} (H) mice, respectively. Each data point represents one individual mouse (n = 5–9).

with inflammatory infiltrates, crypt hyperplasia, and villus destruction (Fig. 3 G). Neutrophil infiltration in the large intestine was also detected by flow cytometry (Fig. 3 H). In addition, we found elevated levels of the inflammatory cytokine IL-23 in the large intestine of zDCΔMHCII, but not in control mice (Fig. 3 I). To confirm that intestinal innate immune responses were intact, we measured the expression of AMPs in the intestine of zDCΔMHCII and control mice. Consistent with the inflammation found in the intestines of these mice, RegIIIγ and S100A9 were found at higher levels in zDCΔMHCII mice compared with controls (Fig. 3 J). ILC3s, whose IL-22 production is crucial for AMP expression (Sonnenberg et al., 2011; Kinnebrew et al., 2012; Satpathy et al., 2013; Bernink et al., 2015), were not affected and actually occurred at higher frequencies in zDCΔMHCII mice compared with controls (Fig. 3 K). We therefore conclude that intestinal inflammation in zDCΔMHCII mice occurs even in the presence of active cDC-dependent innate immune responses.

Normally, intestinal bacteria are separated from epithelial cells by a mucous layer. Innate immune responses and AMPs are essential for this spatial segregation (Vaishnava et al., 2011; Gallo and Hooper, 2012). To visualize bacteria in the large intestine (colon and cecum) of zDCΔMHCII mice and determine their location and proximity to the epithelial barrier, we performed 16S ribosomal RNA (rRNA) fluorescence in situ hybridization (16S FISH). We found that, in zDCΔMHCII mice, intestinal microbes and gut epithelial cells were in direct contact (Fig. 3 L). However, Muc2 expression in the large intestine was unaltered, and therefore zDCΔMHCII mice do not have a defect in mucus production (Fig. 3 M). Finally, neither orally administrated FITC-Dextran nor LPS were detectable at higher levels in the serum of zDCΔMHCII compared with control mice, indicating no gross defect in the epithelial barrier (unpublished data).

A similar phenotype was also observed in CD11cΔMHCII mice (Fig. 4 A) and in zDCΔMHCII, but not control BM chimeras (Fig. 4, B and C). Finally, BM chimeras reconstituted with a 1:1 mixture of control and zDCΔMHCII BM did not develop disease (Fig. 4 C). Therefore, intestinal inflammation in zDCΔMHCII mice is BM cell–dependent and can be rescued by WT BM cells.

Despite the changes in the anatomical distribution of the microbiome in the intestine, we did not observe dramatic differences in the composition of the microbiome (determined by 16S sequencing of fecal bacteria) between control and zDCΔMHCII mice that were cohoused. UniFrac analysis showed that the microbiome in individual mice clustered by the cage in which they were housed and not by genotype, suggesting that the composition of the microbiome is not dramatically altered in zDCΔMHCII mice compared with controls (Fig. 4 D). These data indicate that in addition to AMPs, MHCII expression by cDCs is required to maintain the spatial segregation between microbes and gut epithelial cells.

$CD4^+$ T cell activation is impaired in zDCΔMHCII mice

DCs and thymic epithelial cells are both involved in the selection of mature T cells in the thymus; therefore, we examined thymic $CD4^+$ T cells in zDCΔMHCII mice. Although there was a small increase in mature single-positive $CD4^+$ thymocytes in zDCΔMHCII mice compared with control mice, their Vβ chain usage was comparable (Fig. 5, A and B).

To check for the presence of autoreactive $CD4^+$ T cells in the periphery, we analyzed T cells in the spleen, mLN, and lamina propria of the large intestine for the presence of activated and cytokine-producing $CD4^+$ T cells. zDCΔMHCII mice showed no evidence of increased levels of such cells (Fig. 6). To the contrary, we found reduced frequencies of total $CD4^+$ T cells, as well as increased frequencies of naive $CD4^+$ T cells and reduced frequencies of activated $CD4^+$ T cells, in zDCΔMHCII mice when compared with controls (Fig. 6). In addition, zDCΔMHCII mice showed lower frequencies of peripherally induced regulatory T cells (iT reg cells; defined as $Nrp1^-$) in the mLN and lamina propria of the large intestine compared with controls. This is in accordance with a previously described cDC-mediated feedback mechanism controlling T reg cell numbers (Darrasse-Jèze et al., 2009). Despite reduced iT reg cells, the relative frequency of $CD4^+$ T cells producing IL-2, IL-17, or IFN-γ was comparable or reduced in zDCΔMHCII mice compared with controls (Fig. 6, D–F). This was also confirmed by quantitative PCR (qPCR) analysis of the large intestine, where we found similar expression levels of IL-17 and IFN-γ (Fig. 3 I). Thus, in the absence of MHCII expression by cDCs, the defect in peripheral T reg cell induction did not result in aberrant levels of $CD4^+$ T cell activation.

In contrast to $CD4^+$ T cells, we observed a higher frequency of activated $CD8^+$ T cells ($CD3^+CD8^+CD62L^-CD44^+$) in the spleen and mLN of zDCΔMHCII mice (Fig. 6, D and E). Furthermore, zDCΔMHCII mice showed unaltered or slightly reduced frequencies of γδ T cells in spleen, mLN, and large intestine compared with control mice, ruling out the involvement of pathogenic γδ T cells (Park et al., 2010; not depicted). To investigate whether the phenotype in zDCΔMHCII mice might be a result of insufficient $CD4^+$ T cell activation, we depleted $CD4^+$ T cells in control (MHCII sufficient) mice. Within 4 wk of depletion, mice developed neutrophilia, and elevated levels of Lipocalin-2 were detectable in their feces, although mice did not develop rectal prolapse within the 4 wk of depletion (Fig. 7 A; and not depicted). To test whether the observed increase in activated $CD8^+$ T cells contributed to the phenotype in zDCΔMHCII mice, we depleted $CD8^+$ T cells for 4 wk. However, $CD8^+$ T cell–depleted zDCΔMHCII mice did not differ from nondepleted zDCΔMHCII mice (Fig. 7 B). Collectively, these data suggest that the phenotype in zDCΔMHCII mice is associated with insufficient adaptive $CD4^+$ T cell responses but not pathogenic γδ or $CD8^+$ T cells.

Microbiota is required for intestinal inflammation

To test the possibility that zDCΔMHCII mice develop intestinal inflammation as a result of inefficient effector $CD4^+$ T

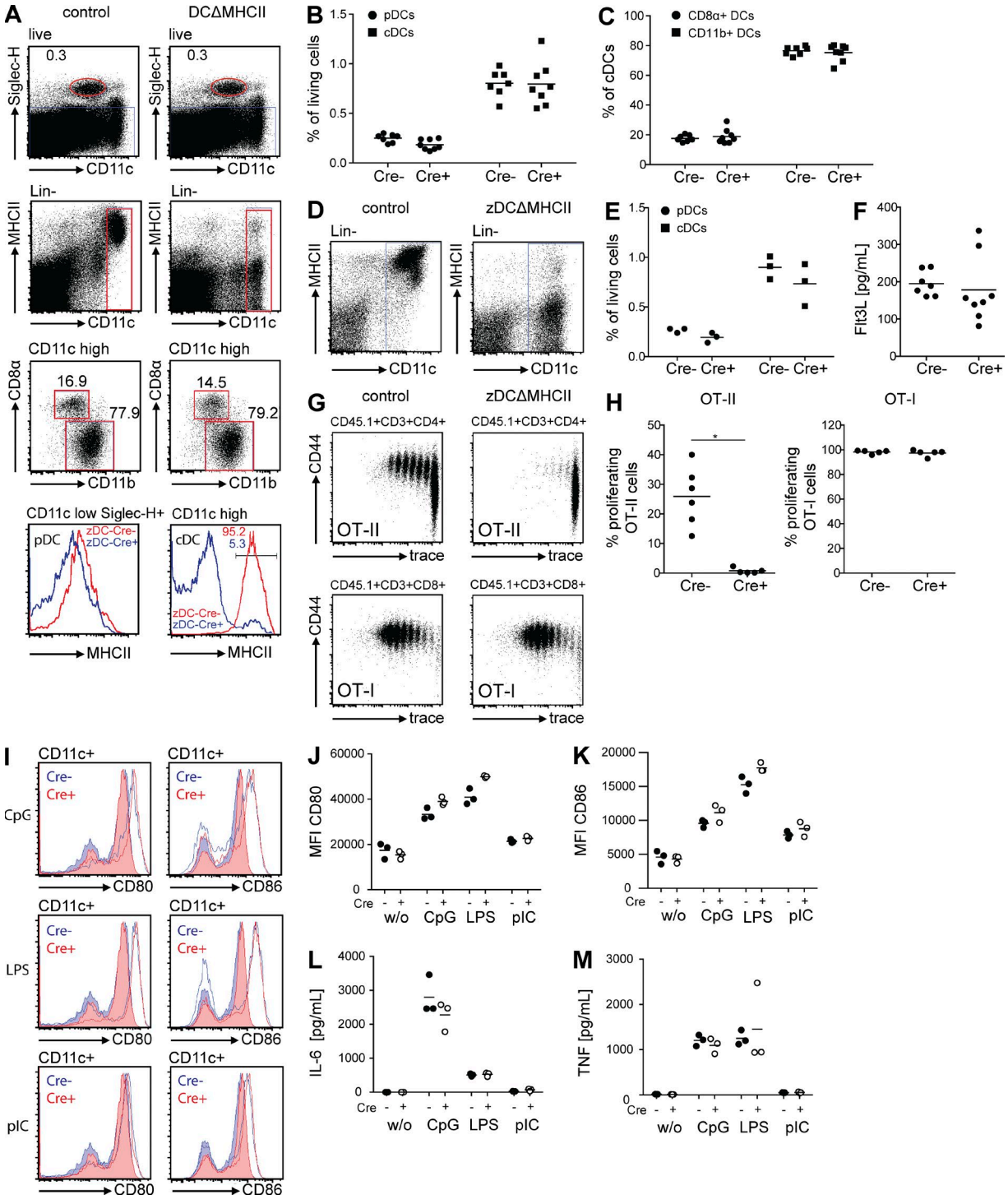

Figure 2. **zDCΔMHCII mice.** (A) Flow cytometric analysis of splenocytes from control and zDCΔMHCII mice. Histograms depict expression of MHCII on the cell surface of cDCs ($Lin^{-}CD11c^{high}$) and pDCs ($CD11c^{low}Siglec\text{-}H^{+}$). (B) Graph depicts frequency of pDCs and cDCs among living splenocytes. (C) Graph depicts ratio of $CD8\alpha^{+}$ and $CD11b^{+}$ cDCs. Each data point represents one individual mouse (n = 7–8). (D) Flow cytometric analysis of mLN cells from control and zDCΔMHCII mice. Dot plots depict expression of MHCII on the cell surface of cDCs ($Lin^{-}CD11c^{high}$). (E) Graph depicts frequency of pDCs and cDCs among living mLN cells. Each data point represents one individual mouse (n = 3). (F) Serum levels of Flt3L. Each data point represents one individual mouse (n = 7–8). (G and H) OT-II (top row) or OT-I (bottom row) T cells were transferred into control and zDCΔMHCII mice, respectively. Mice were immunized (i.p.) with 100 µg OVA + 10 µg pIC. Proliferation was analyzed 3 d later. (G) Dot plots show proliferation and CD44 expression of OT-II (top row) and OT-I (bottom row) T cells in LNs (pooled mesenteric and inguinal LN). (H) Graph depicts percentage of OT-II (left) and OT-I (right)

cell responses to intestinal bacteria, we treated the mice with broad-spectrum antibiotics. Lipocalin-2 in the feces, Csf3 in serum, and neutrophil levels in the spleen of zDCΔMHCII mice dropped to baseline levels after 4 wk of antibiotic treatment (Fig. 8, A–C). Consistent with these findings, antibiotic-treated zDCΔMHCII mice were free of intestinal inflammation and inflammatory infiltrate as determined by histology (Fig. 8 E). Moreover, maintaining zDCΔMHCII mice in a germ-free environment completely prevented the development of all signs of disease, including intestinal inflammation, high levels of Lipocalin-2, elevated Csf3 levels, neutrophilia, and increased numbers of activated $CD8^+$ T cells (Fig. 8, A–E). These results indicate that the intestinal inflammation in zDCΔMHCII mice is dependent on the microbiota. They also suggest that rather than causing the disease, the activated $CD8^+$ T cells in specific pathogen–free (SPF) zDCΔMHCII mice develop in response to microbiota-mediated inflammation.

zDCΔMHCII mice exhibit impaired antimicrobial adaptive immune responses

IgA, the most abundant antibody isotype at mucosal surfaces, is secreted into the intestinal lumen, where it coats bacteria that enter the host and elicit adaptive immune responses (Palm et al., 2014). mLNs, Peyer's patches (PPs), and isolated lymphoid follicles are the primary sites of adaptive immune responses against intestinal antigens. zDCΔMHCII mice showed normal levels of B cells in the mLNs, PPs, and lamina propria of the large intestine. Whereas GC B cells were reduced in zDCΔMHCII mice, the relative frequency of IgA^+ B cells was not; the only significant defect in this compartment was in the lamina propria, suggesting that zDCΔMHCII mice do not have an overall defect in class switching. Consistent with the relative paucity of GC B cells, zDCΔMHCII mice showed significantly reduced frequencies of follicular T helper (TFH) cells in both mLNs and PPs (Fig. 9, A–D). These results support the idea that zDCΔMHCII mice have aberrant antimicrobial adaptive immune responses due to insufficient $CD4^+$ T cell help (Grajales-Reyes et al., 2015).

To directly measure adaptive immune responses against intestinal bacteria, we colonized germ-free control and zDCΔMHCII mice with a mixture of six different commensal intestinal bacteria (*Escherichia coli*, *Enterococcus faecalis*, *Bifidobacterium longum*, *Lactobacillus plantarum*, *Bacteroides vulgatus*, and *Ruminococcus gnavus*). Colonization was similar for control and zDCΔMHCII mice as determined by PCR 8 wk after colonization (Fig. S2). Although germ-free mice have no detectable GC B or TFH cells in gut-associated lymphoid tissues, newly colonized control mice showed robust GC B and TFH cell responses in mLNs and PPs. In contrast, these responses were barely detectable in colonized zDCΔMHCII mice, even 8 wk after colonization (Fig. 10, A and B).

Consistent with the near absence of GC responses, IgA levels in the feces and serum of colonized zDCΔMHCII mice were significantly lower compared with colonized control mice. Fecal IgA increased progressively in control mice starting after day 7, reaching a mean of 200–400 ng/mg feces. In contrast, fecal IgA reached a plateau of around 10–20 ng/mg feces by day 12 and remained relatively constant thereafter in zDCΔMHCII mice (Fig. 10, C and D). Consistent with the overall lower levels of serum and fecal IgA, bacteria isolated from feces of zDCΔMHCII mice were coated with far lower levels of IgA than bacteria from feces of control mice (Fig. 10 E).

Collectively, these data reveal that zDCΔMHCII mice have defective adaptive immune responses against intestinal commensals, and this defect is associated with a loss of bacterial segregation from the epithelium and severe colitis.

DISCUSSION

cDCs link innate and adaptive immunity by sensing pathogens and initiating adaptive immune responses. Although the two physiological functions of cDCs are likely to play distinct roles in immune homeostasis, they have not previously been evaluated independently. In the gut, cDCs sense and capture gut microbes in part by extending their processes into the gut lumen (Macpherson and Uhr, 2004; Niess et al., 2005; Chieppa et al., 2006; Vallon-Eberhard et al., 2006). Microbial sensing induces cDCs to produce cytokines such as IL-23, which are required to activate innate lymphoid cells (Kinnebrew et al., 2012; Satpathy et al., 2013). In addition, the ingested microbes are carried to local lymphoid organs, such as the mLNs, processed, and presented to T cells to initiate adaptive immune responses (Macpherson and Uhr, 2004; Niess et al., 2005).

Ablation experiments using $CD11c^{DTR}$ mice, conditional deletion of genes (e.g., *Irf4*, *Irf8*, or *Notch2*) with $CD11c^{Cre}$ mice, and *Batf3*-deficient mice result in loss of cDCs and cDC subsets, and therefore concomitant loss of both innate and adaptive immune functions (Hildner et al., 2008; Lewis et al., 2011; Persson et al., 2013; Schlitzer et al., 2013). For example, $CD11c^{Cre}$-mediated DC deletion has been described to activate a feedback loop that produces high levels of circulating Flt3L, resulting in a myeloproliferative syndrome characterized by extramedullary hema-

cells that proliferated in response to OVA + pIC. Each data point represents one individual mouse (n = 5–6). (I–M) cDCs were isolated from spleens of control and zDCΔMHCII mice. 250,000 cells were incubated with 1 µM CpG 1668, 1 µg/ml LPS, and 1 µg/ml pIC. 16 h later, expression of CD80 and CD86 was determined by flow cytometry. Cytokines produced by cDCs after stimulation were measured in the supernatant. *, $P < 0.05$. (I) Histograms show expression of CD80 and CD86 on cDCs. Filled histograms show expression of CD80 and CD86 on unstimulated cells. Open histograms show levels of CD80 and CD86 after stimulation. (J and K) Graphs depict levels of expression (MFI) of CD80 and CD86 on cDCs. (L and M) Graphs depict production of IL-6 and TNF by cDCs. n = 3.

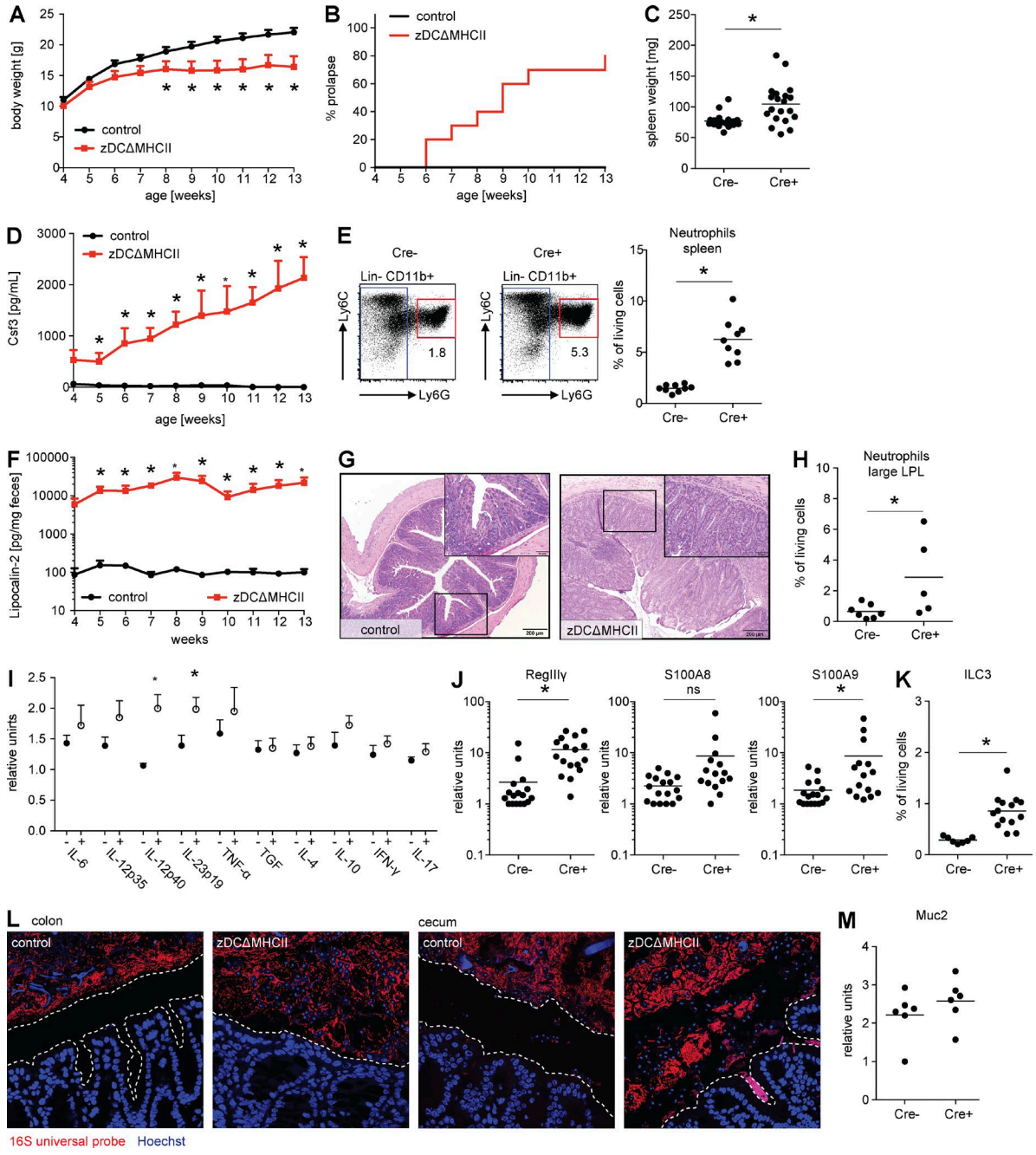

Figure 3. **zDCΔMHCII mice develop severe intestinal inflammation.** (A) Graph depicts absolute body weight of control (black line) and zDCΔMHCII mice (red line) in grams, starting at 4 wk of age. Shown is the mean + SEM (n = 10–12). (B) Graph depicts the frequency of mice that developed rectal prolapse. Control (black line) and zDCΔMHCII mice (red line; n = 10–12). (C) Graph depicts total weight of spleen in milligrams. Each data point represents one individual mouse (n = 19–20). (D) Graph depicts concentration of Csf3 in the serum of control (black line) and zDCΔMHCII mice (red line) as the mean + SEM (n = 10–12). (E) Flow cytometric analysis of splenocytes from control and zDCΔMHCII mice. Numbers in dot plots show frequency of neutrophils ($Lin^{-}CD11b^{+}Ly6C^{low}Ly6G^{+}$) among living cells. Graph depicts frequency of neutrophils among living cells. Each data point represents one individual mouse (n = 9). (F) Graph depicts concentration of Lipocalin-2 in the feces of control (black line) and zDCΔMHCII mice (red line) as the mean + SEM (n = 10–12). (G) Histopathological analysis of the large intestine of control (left) and zDCΔMHCII mice (right) that were maintained under SPF conditions. The large inset represents enlarged view of small inset and shows cellular infiltrates. (H) Graph depicts frequency of neutrophils among living cells in the lamina propria of the large intestine. Each data point represents one individual mouse (n = 5–7). (I) Expression of cytokines in the large intestine (whole tissue) was determined by qPCR. Graph depicts expression as relative units. Each data point represents one individual mouse (n = 5). (J) Expression of RegIIIγ, S100A8, and S100A9 in epithelial cells isolated from the small intestine was determined by qPCR. Graphs depict expression as relative units. Each data point represents one individual mouse (n = 15–17). (K) Graph depicts frequency of ILC3s ($CD45^{+}/CD19^{-}/B220^{-}/NK1.1^{-}/Gr1^{-}/CD3^{-}/Thy1.2^{+}/ROR\gamma t^{+}$) among living cells in the

topoiesis, splenomegaly, and neutrophilia (Birnberg et al., 2008). Depletion of cDCs in this model likely has additional consequences beyond elevated Flt3L levels. Our data suggests that the phenotype may have been mediated in part by intestinal microbes. In a different study, however, $CD11c^{Cre}$-mediated DC depletion was associated with colitis and increased numbers of activated $CD4^+$ T cells (Birnberg et al., 2008; Ohnmacht et al., 2009). Although cDCs play an important role for T cell selection in the thymus (Perry et al., 2014), in our model we found no evidence of activated or autoreactive $CD4^+$ T cells. In addition to being unable to distinguish between the innate and adaptive functions of cDCs, interpretation of these earlier studies was confounded in part by deletion of CD11c expressing monocytes, macrophages, pDCs, and NK cells. In contrast, deletion of MHCII in cDCs using zDC^{Cre} selectively ablates the ability of this cell type to initiate adaptive immunity while leaving its innate activity intact. The described phenotype was specific for cDCs because zDC expression is restricted to cDCs and their precursors. zDC is first expressed in committed cDC progenitors (pre-DCs) in the BM and is maintained in all subsequent stages of cDC development, including all major subsets of cDCs (Meredith et al., 2012; Satpathy et al., 2012).

Our experiments show that cDC-induced adaptive immune responses are required to maintain homeostasis between intestinal flora and the host. Other MHCII-expressing antigen-presenting cells, such as activated monocytes, macrophages, or monocyte-derived DCs, are unable to compensate for this requirement, because they are not specialized for $CD4^+$ T cell priming. Absence of MHCII on cDCs in zDCΔMHCII mice is associated with intestinal inflammation and elevated serum levels of Csf3, an acute phase reactant. This phenotype is dependent on bacteria, as Csf3 levels dropped to normal levels when the mice were treated with antibiotics or housed under germ-free conditions. These results highlight a previously underappreciated role for cDC-mediated adaptive immune responses to commensal bacteria. Mice lacking MHCII on cDCs may therefore be considered immunocompromised, as they are unable to efficiently prime $CD4^+$ T cells. Consistent with our observations, mice lacking $CD4^+$ T cells and HIV-infected humans that suffer $CD4^+$ T cell loss show increased microbial translocation and systemic immune activation (Brenchley et al., 2006; Sandler and Douek, 2012).

cDC-initiated $CD4^+$ T cell responses are likely to help keep the gut microbiome in check by at least several distinct mechanisms. They are required to activate and induce differentiation of T cells, such as protective TH17/TH22 cells, which prevent invasion of enterobacteria (Mangan et al., 2006; Curtis and Way, 2009; Ivanov et al., 2009; Basu et al., 2012). Consistent with this idea, T cell–deficient mice and humans show increased risk for intestinal inflammation (Tamura et al., 2005). In addition, cDCs are also essential in initiating TFH responses that are required to produce germinal centers and high-affinity IgA (Crotty, 2011; Maruya et al., 2013; Kato et al., 2014; Kubinak et al., 2015). Finally, MHCII expression by cDC is required to maintain the physiological number of induced T reg cells (Darrasse-Jèze et al., 2009). In zDCΔMHCII mice, reduced numbers of T reg cells did not result in increased numbers of activated $CD4^+$ T cells because their activation requires MHCII expression on cDCs. Nevertheless, decreased numbers of induced T reg cells could contribute to the severity of the phenotype by altering innate immune responses.

Colonization of germ-free mice allowed us to follow the immune response against a limited number of commensal bacteria. This controlled experiment showed that zDCΔMHCII mice have diminished TFH, GC, and IgA responses to intestinal bacteria. Mice that are unable to secrete polymeric antibodies into the intestinal lumen show elevated serum IgG levels specific for commensal bacteria, suggesting more translocation of intestinal bacteria in the absence of luminal IgA (Johansen et al., 1999). In addition, translocation of bacteria was observed in germ-free B cell–deficient mice that were colonized with SPF microbiota (Macpherson and Uhr, 2004), emphasizing the importance of the adaptive response in containing the microbiota. However, the phenotype observed in zDCΔMHCII mice cannot be mediated solely by a defective IgA response against intestinal bacteria. $AID^{-/-}$ mice, which are unable to switch to IgA, do not develop the phenotype in our SPF facility, possibly because they have unimpaired TFH and germinal center responses and IgM can compensate in part for IgA. In $zDC^{Cre+}MHCII^{fl/fl}$ mice, however, $CD4^+$ TFH cell priming is defective, resulting in diminished GCs. This idea is supported by the observation that $CD4^+$ T cell depletion partially phenocopies $zDC^{Cre+}MHCII^{fl/fl}$ mice.

cDCs in zDCΔMHCII mice show intact innate microbial sensing and cytokine production. These features are essential for activation and normal function of innate lymphoid cells (Bernink et al., 2015). The observation that zDCΔMHCII mice develop intestinal inflammation indicates that intact innate mechanisms are insufficient to maintain the normal balance between host and intestinal commensals. Transferable risk for colitis has been described for mice lacking components of the inflammasome, which has been attributed to alterations in intestinal microbiota (Elinav et al., 2011; Palm et al., 2014).

lamina propria of the small intestine. (L) Pictures show localization of bacteria (red) and epithelial cells (blue) visualized by 16S FISH and Hoechst staining in the colon (left) and the cecum (right). Dotted line outlines the space between epithelial cells and luminal content. (M) Expression of Muc2 in epithelial cells isolated from the large intestine was determined by qPCR. Graph depicts expression as relative units. Each data point represents one individual mouse ($n = 6$). If not stated otherwise, mice analyzed were 8–12 wk old. *, $P < 0.05$

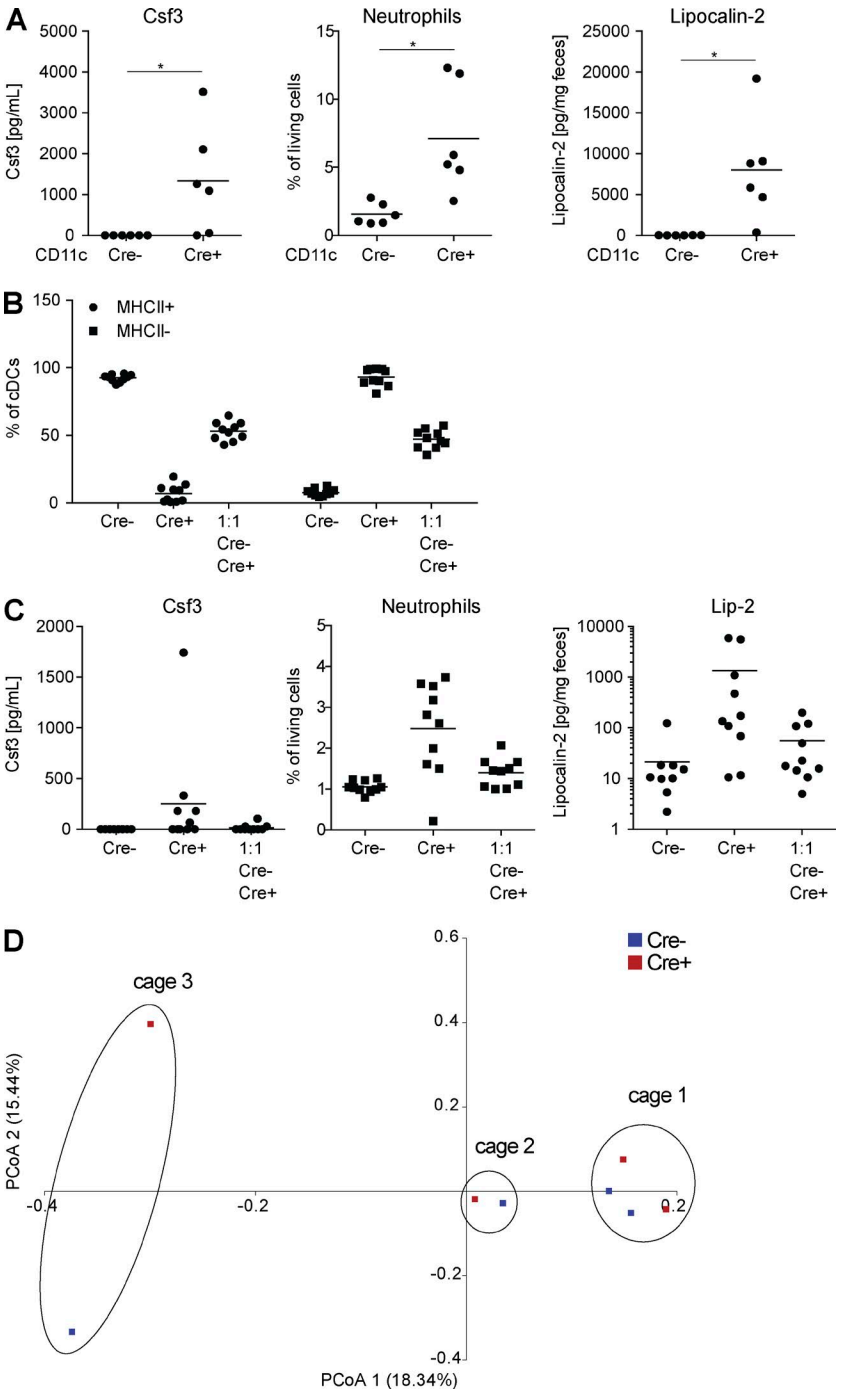

Figure 4. **CD11cΔMHCII mice, zDCΔMHCII BM chimeras, and microbiome in zDCΔMHCII mice.** (A) Graphs depict serum levels of Csf3, frequency of neutrophils among living cells in the spleen, and concentration of Lipocalin-2 in the feces of control and CD11cΔMHCII mice. Each data point represents one individual mouse ($n = 6$). Mice were analyzed at the age of 6–8 wk. (B and C) WT B6 mice were irradiated and reconstituted with BM from control or zDCΔMHCII mice. A third group received a 1:1 mix of BM from control and zDCΔMHCII mice. (B) Graph depicts percentage of cDCs expressing MHCII. (C) Graphs depict serum levels of Csf3, frequency of neutrophils among living cells in the spleen and concentration of Lipocalin-2 in the feces of mice reconstituted with BM from control, zDCΔMHCII mice, or a 1:1 mix of BM from control and zDCΔMHCII mice, respectively. Each data point represents one individual mouse ($n = 10$). Mice were analyzed 10 wk after irradiation. *, $P < 0.05$. (D) Feces was collected from control and zDCΔMHCII mice (10–12 wk old) and microbial composition was analyzed by 16S rRNA sequencing. UniFrac analysis is shown. Cage numbers indicate which mice were cohoused in the same cage.

In our experiments, control mice did not develop any signs of inflammation, although they were cohoused with zDCΔMHCII mice. The fact that cohoused control mice did not get sick, along with the finding that they share a similar microbiome, indicates that commensal bacteria that can be controlled and are usually harmless in mice with an unimpaired immune system may be responsible for disease in zDCΔMHCII mice that have defective adaptive immune responses. Collectively, the data indicate that in the steady state, cDC-mediated $CD4^+$ T cell priming and subsequent adaptive immune responses are essential to maintain homeostasis and prevent intestinal commensals from producing pathology.

MATERIALS AND METHODS

Mice. zDC^{Cre} knock-in mice were generated by homologous recombination in C57BL/6 albino embryonic stem cells at The Rockefeller University Gene Targeting Resource Cen-

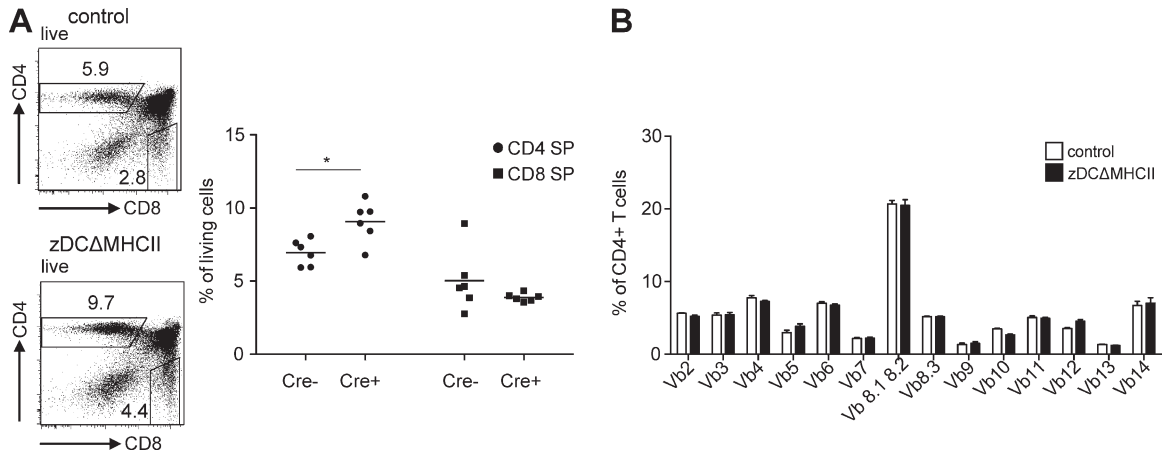

Figure 5. **Thymic CD4⁺ T cells.** (A) Flow cytometric analysis of thymocytes from control and zDCΔMHCII mice. Numbers in dot plots show frequency of single-positive CD4 and CD8 thymocytes, respectively. Graph depicts frequency of single-positive CD4 and CD8 thymocytes of living cells. Each data point represents one individual mouse ($n = 6$). (B) Graph depicts TCR repertoire of CD4⁺ T cells in the spleen and Vβ chain usage in control and zDCΔMHCII mice as means + SEM ($n = 7$). *, $P < 0.05$.

ter (NewYork, NY). The targeting strategy was the same as for the previously described zDC^{DTR} mice (Meredith et al., 2012). zDC^{Cre} mice were maintained on a C57BL/6 background. *Itgax*^{Cre} (CD11c^{Cre}; stock number 008068), *Rosa26*^{lSlYFP} (Rosa26^{lSlYFP}; stock number 006148), *iab*^{neo} (MHCII$^{fl/fl}$; stock number 013181), and *Irf4*$^{fl/fl}$ (IRF4$^{fl/fl}$; stock number 009380) mice were purchased from The Jackson Laboratory. Mice were housed in The Rockefeller University Comparative Bioscience Center (New York, NY) under SPF and germ-free conditions, respectively. All experiments were performed in accordance with the National Institutes of Health guidelines and approved by The Rockefeller University Animal Care and Use Committee. Germ-free mice were obtained by transfer of newborn pups (Cesarean section) into germ-free isolators. Germ-free status was confirmed by plating feces on a broad range of nutrient agars, as well as by qPCR analysis (16S rRNA). zDCΔMHCII mice were bred with MHCII$^{fl/fl}$ mice. This way we could compare Cre$^+$ (zDCΔMHCII) and Cre$^-$ (control) littermates. It is also important to note that zDCΔMHCII males were bred with MHCII$^{fl/fl}$ females. This way, the fostering female is healthy and does not develop the described phenotype, and development of pups is not affected by the genotype of the fostering female. Littermates were cohoused during all experiments. Mice were generally analyzed at 8–12 wk of age.

BM chimeras. BM chimera recipients were irradiated with two doses of 525 rad 3 h apart and injected with 5–10 × 10^6 BM cells. BM chimeras were analyzed 10 wk after irradiation.

Flow cytometry and cell sorting. For FACS analysis, cells were stained using antibodies against B220 (RA3-6B2), BST2 (eBio927), CXCR5 (L138D7), F4/80 (BM8), Foxp3 (FJK-16s), Gr-1 (RB6-8C5), IFN-γ (181157), IL-2 (JES6-5H4), IL-17A (TC11-18H10), Ly6C (AL-21), Ly6G (1A8), MHCII (M5/114.15.2), NK1.1 (PK136), Nrp1 (3DS304M), PD-1 (J43), RORg(t) (B2D), Siglec-H (440c), TCRβ (H57-597), CD3 (145-2C11), CD4 (RM4-5), CD8 (53–6.7), CD11b (M1/70), CD11c (N418), CD19 (1D3), CD38 (90), CD44 (1M7), CD45 (30-F110), CD62L (MEL-14), CD64 (X54-5/7.1), CD95 (Jo2), CD103 (2E7), CD115 (AFS98), TCRγδ (GL3), CD80 (16-10A1), and CD86 (GL1). TCR Vβ chain distribution was assessed with a FITC-labeled screening panel (BD). PI (Sigma-Aldrich), DAPI (Invitrogen), or Aqua live/dead (Invitrogen) was added to exclude dead cells from analysis. For intracellular cytokine staining, cells were stimulated for 4 h using Leukocyte Activation Cocktail with GolgiPlug (BD). Surface stained cells were fixed with Cytofix/Cytoperm (BD) and washed with Perm/Wash buffer (BD). Cells were analyzed on a LSR Fortessa flow cytometer (BD). Analysis was performed using FlowJo software (Tree Star).

Spleen, LN, thymus, and PP cell isolation. For isolation of mononuclear phagocytes, spleen and LNs were mechanically disrupted and incubated with HBSS (Gibco) + 5% FBS + 0.5 mg/ml Collagenase D (Roche) at 37°C for 30 min. Cells were filtered through 100 µM cell strainers and washed. Erythrocytes were lysed with ACK Lysing buffer (Gibco). For isolation of T and B cells, spleen, LNs, thymi, and PP were mechanically disrupted, filtered through 100-µM cell strainers, and washed. Erythrocytes were lysed with ACK Lysing buffer (Gibco).

In vitro stimulation of DCs. 250,000 cDCs (CD11c MACS enrichment) were stimulated with 1 µM CpG 1668, 1 µg/ml LPS, and 1 µg/ml pIC, respectively. Expression of CD80 and CD86 were determined by flow cytometry 16 h later. Cytokines were measured using the Cytometric Bead Array kit (BD).

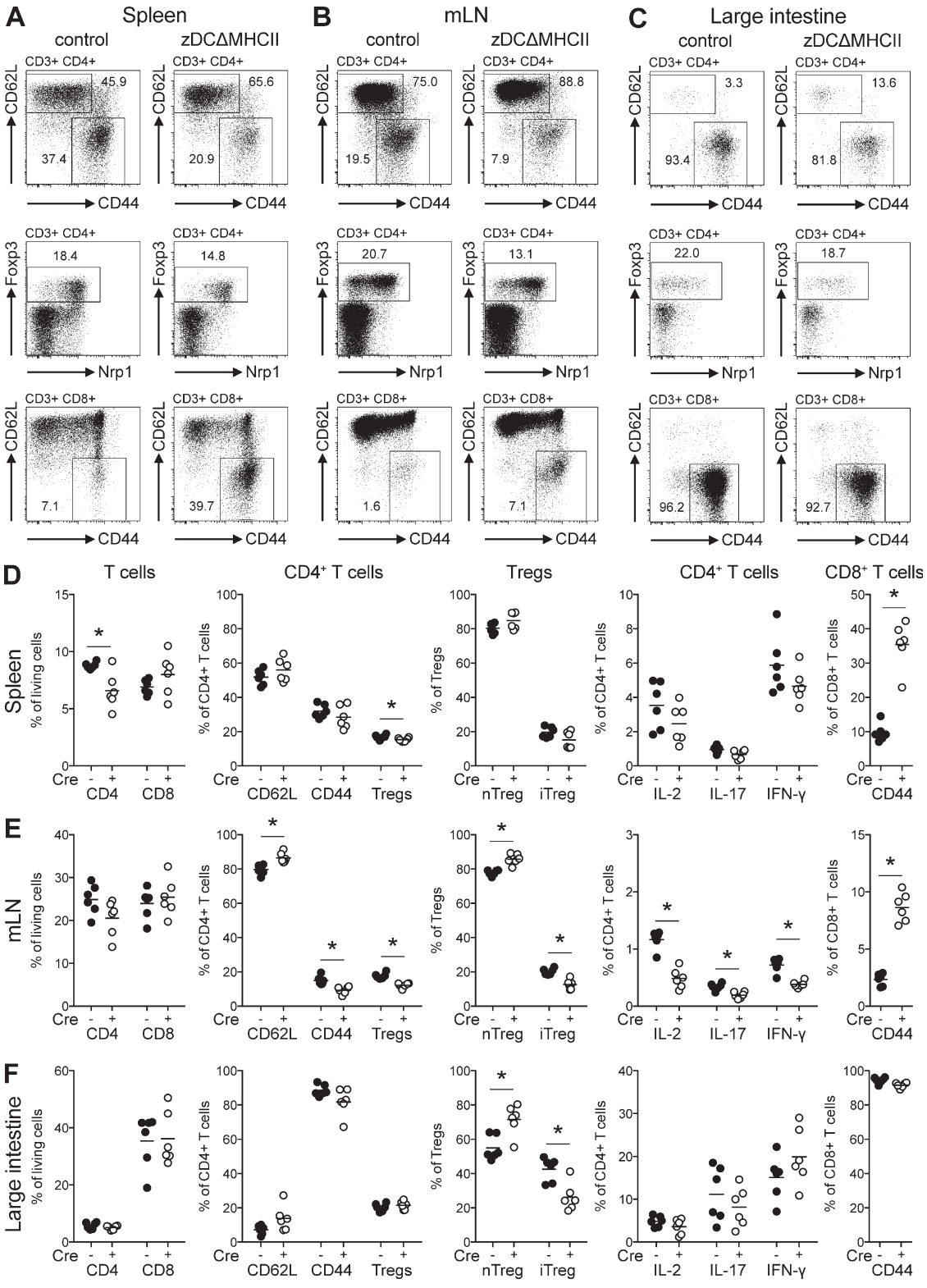

Figure 6. **CD4⁺ T cells in zDCΔMHCII mice are not autoreactive.** Frequency and phenotype of CD4⁺ and CD8⁺ T cells in control and zDCΔMHCII mice, respectively. Dot plots show ratio of naive (CD62L⁺) and activated (CD44⁺) CD4⁺ and CD8⁺ T cells and percentage of CD4⁺ T reg cells (Foxp3⁺) in spleen (A), mLN (B), and large intestine (C) lamina propria. Graphs depict frequency of CD4⁺ and CD8⁺ T cells among living cells, frequency of CD62L⁺, CD44⁺, and

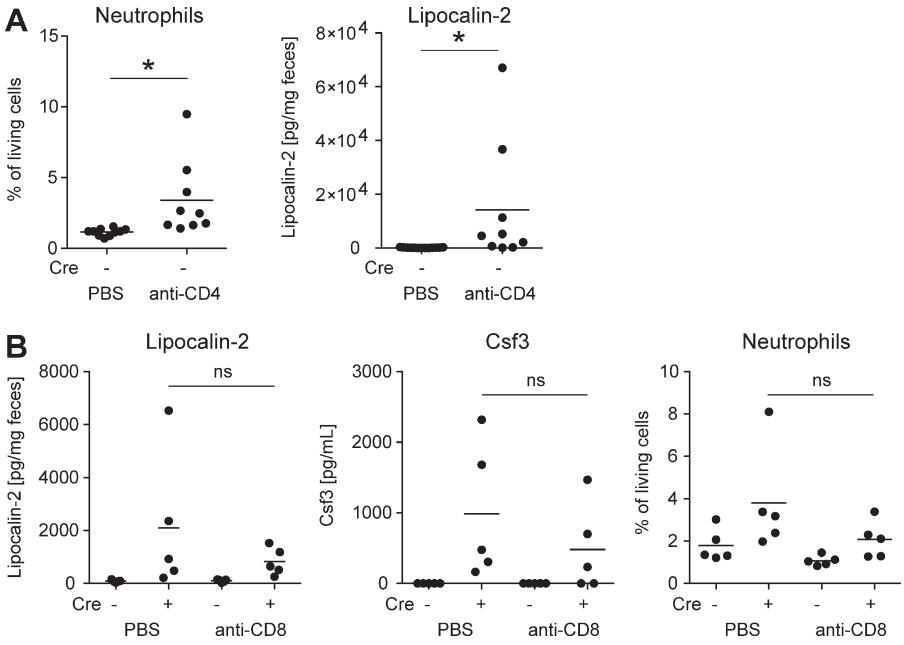

Figure 7. **CD4$^+$ T cell depletion induces neutrophilia and intestinal inflammation.** CD8$^+$ T cell depletion does not affect disease. (A) Cre$^-$ control mice were injected with PBS or 100 µg anti-CD4 antibody (clone GK1.5) every 2–3 d for 4 wk. Graphs depict frequency of neutrophils among living cells in the spleen and concentration of Lipocalin-2 in the feces. Each data point represents one individual mouse (n = 9–13). (B) Cre$^-$ control and zDCΔMHCII mice were injected with PBS or 100 µg anti-CD8 antibody (clone 53–6.72) every 2–3 d for 4 wk. Graphs depict concentration of Lipocalin-2 in the feces, serum levels of Csf3, and frequency of neutrophils among living cells in the spleen. Each data point represents one individual mouse (n = 5). *, P < 0.05.

Intestinal cell isolation. Small and large intestine were excised and freed of mesentery and fat. Feces were removed and PPs were excised from the small intestine. Both small and large intestine were opened longitudinally and washed in HBSS, followed by HBSS + 1 mM DTT (Sigma-Aldrich). Tissue was cut into 1-cm pieces and incubated with 25 ml of HBSS + 5% FBS + 5 mM EDTA for 15 min at 37°C at 230 rpm. Supernatant containing intraepithelial lymphocytes was decanted and spun down (for RNA isolation from epithelial cells, see next section). Tissue was washed with 10 ml of HBSS + 5% FBS for 15 min at 37°C at 230 rpm. The gut tissues were then finely chopped and digested in HBSS + 5% FBS + 1X Sodium Pyruvate + 25 mM Hepes + 50 µg/ml DNaseI + 0.05 mg/ml Collagenase VIII for 1 h at 37°C at 100 rpm. Cells were separated by discontinuous Percoll gradient (70%/35%) centrifugation. Cells were isolated from the interphase.

RNA isolation and qPCR. Epithelial cells were resuspended in TRIzol (Invitrogen), RNA was isolated according to the manufacturer's protocol, and cDNA was generated using Superscript II (Invitrogen) and random primers. GAPDH forward, 5′-CTACAGCAACAGGGTGGTGG-3′, GAPDH reverse, 5′-AGATGGGGCATCTTTCTTGG-3′; S100A8 forward, 5′-TGCGATGGTGATAAAAGTGG-3′, S100A8 reverse, 5′-GGCCAGAAGCTCTGCTACTC-3′; S100A9 forward, 5′-CACCCTGAGCAAGAAGGAAT-3′, S100A9 reverse, 5′-TGTCATTTATGAGGGCTTCATTT-3′; Muc2 forward, 5′-ACAAAAACCCCAGCAACAAG-3′, Muc2 reverse, 5′-GAGCAAGGGACTCTGGTCTG-3′. All qPCR reactions were performed with Brilliant SYBR Green (Agilent Technologies) on an Mx3005P system (Agilent Technologies).

ELISA. Serum levels of Flt3L and Csf3 were determined by ELISA (R&D Systems) according to the manufacturer's protocol. Lipocalin-2 levels were measured in feces by ELISA according to the manufacturer's protocol (R&D Systems). IgA concentrations were determined by ELISA according to the manufacturer's protocol (eBioscience).

Histology. Tissue was fixed in 10% Formalin. Tissue was embedded, cut, and stained by the Tri-Institutional Laboratory of Comparative Pathology (New York, NY). A pathologist evaluated the tissue sections in a blinded fashion and took pictures representing the phenotype of the respective group.

OT-I and OT-II T cell transfer. CD8$^+$ and CD4$^+$ T cells were isolated from spleen and LNs of CD45.1$^+$ OT-I and OT-II mice, respectively (MACS enrichment), labeled with violet tracem, and transferred into control and zDCΔMHCII mice (CD45.2) by i.v. injection (3–5 × 10^6 cells/mouse). Mice were immunized (i.p.) with 100 µg OVA + 10 µg pIC. 3 d later, proliferation and expression of activation

Foxp3$^+$ cells among CD4$^+$ T cells, frequency of natural (Nrp1$^+$) and induced (Nrp1$^-$) T reg cells among Foxp3$^+$ cells, frequency of cytokine producing CD4$^+$ T cells, and frequency of CD62L$^-$CD44$^+$ cells among CD8$^+$ T cells in spleen (D), mLN (E), and large intestine (F) lamina propria. Each data point represents one individual mice (n = 6). Mice analyzed were 14 wk old. *, P < 0.05.

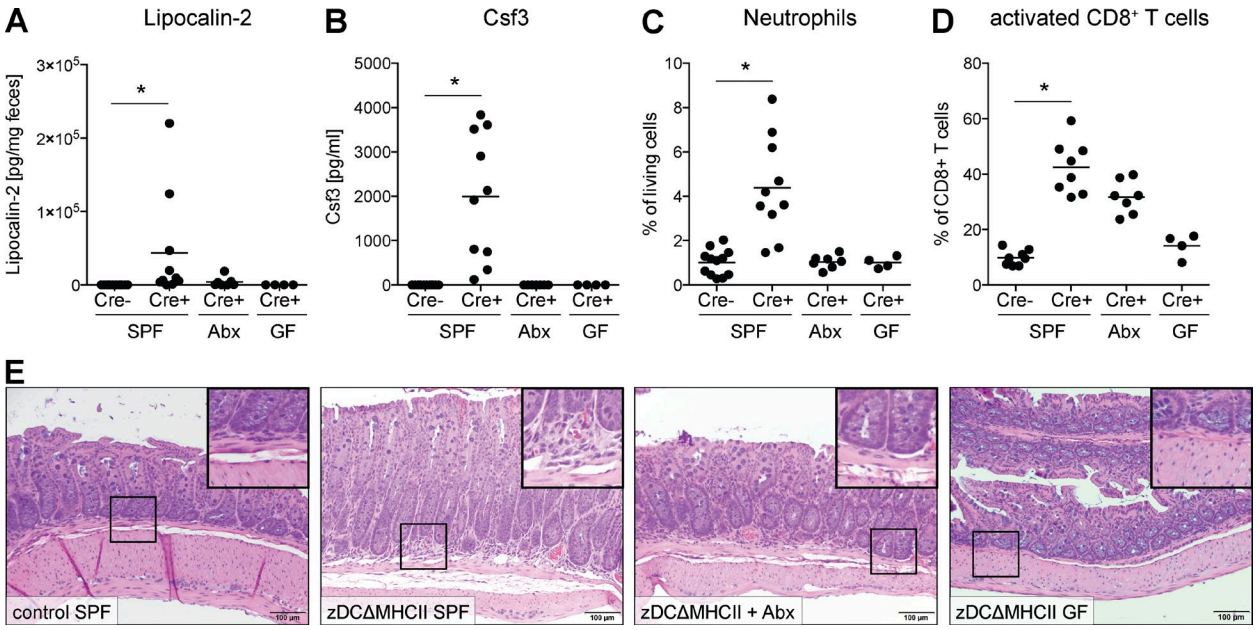

Figure 8. **Treatment of zDCΔMHCII mice with antibiotics reduces intestinal inflammation.** (A) Graph depicts concentration of Lipocalin-2 in the feces of control and zDCΔMHCII mice that were maintained under SPF conditions, zDCΔMHCII mice that received antibiotics with the drinking water for 4 wk, and zDCΔMHCII mice that were maintained under germ-free conditions. Each data point represents one individual mouse (n = 4–12). (B) Graph depicts serum levels of Csf3. Each data point represents one individual mouse (n = 4–12). (C) Graph depicts frequency of neutrophils among living cells in the spleen. Each data point represents one individual mouse (n = 4–12). (D) Graph depicts frequency of $CD62L^{-}CD44^{+}$ cells among $CD8^{+}$ T cells in the spleen. Each data point represents one individual mouse (n = 4–8). (E) Histopathological analysis of the large intestine of control and zDCΔMHCII mice that were maintained under SPF conditions, zDCΔMHCII mice that received antibiotics in the drinking water for 4 wk, and zDCΔMHCII mice that were maintained under germ-free conditions. Large inset represents enlarged view of small inset and shows cellular infiltrates. *, $P < 0.05$.

markers was analyzed by flow cytometry (pooled mesenteric and inguinal LN).

$CD4^{+}$ and $CD8^{+}$ T cell depletion. To deplete $CD4^{+}$ T cells, mice were injected i.p. with 100 µg anti-CD4 (GK1.5; Bio X Cell) every 2–3 d for 4 wk. To deplete $CD8^{+}$ T cells mice were injected i.p. with 100 µg anti-CD8 (53–6.72; Bio X Cell) every 2–3 d for 4 wk.

Abx treatment. Ampicillin (1 mg/ml), Neomycin (1 mg/ml), Vancomycin (0.5 mg/ml), and Metronidazole (1 mg/ml; Sigma-Aldrich) were administered in the drinking water. Mice were put on Abx drinking water at the age of 8–10 wk and kept on Abx for 4 wk.

Time course/aging experiments. Body weight was measured weekly, as well as occurrence of rectal prolapse. Feces and serum samples were collected and stored at −20°C until further use.

16S FISH. 16S rRNA FISH was performed with a universal probe (EUB388; Cy3-GCTGCCTCCCGTAGGAGT-Cy3) on sections fixed with Methacarn solution as described previously (Salzman et al., 2002; Swidsinski et al., 2005). In brief, intestinal tissues (~1 cm), including intestinal contents, were fixed in Methacarn solution (60% methanol, 30% chloroform, and 10% glacial acetic acid) for 6 h at 4°C. After three washes with 70% ethanol, tissues were embedded in paraffin. 5-µm sections were cut and deparaffinized with xylene, and subsequently dehydrated. Probe was diluted (5 ng/µl) in hybridization buffer (0.9 M NaCl, 20 mM Tris-HCl, pH 7.2, and 0.1% SDS), and hybridization was performed at 50°C for 3 h in. After hybridization, tissues were washed with wash buffer (0.9 M NaCl and 20 mM Tris-HCl, pH 7.2) and nuclei were stained with Hoechst stain.

Bacteria isolation and IgA staining. Bacteria were isolated from feces as described previously (Palm et al., 2014). Coating of bacteria with endogenous IgA was determined by staining bacteria with anti–mouse-IgA-PE (clone mA-6E1). Where indicated, MFIs were normalized to the sample with the lowest MFI to be able to compare different time points.

DNA extraction, V4–V5 16S rRNA gene amplification, multiparallel sequencing, and sequence analysis. Fecal samples and intestinal contents were frozen immediately after collection in a dry ice/ethanol slurry and stored at −80°C. DNA was extracted using the phenol-chloroform and bead beating method described previously (Ubeda et al., 2010). The V4-V5 region of the 16S rRNA gene

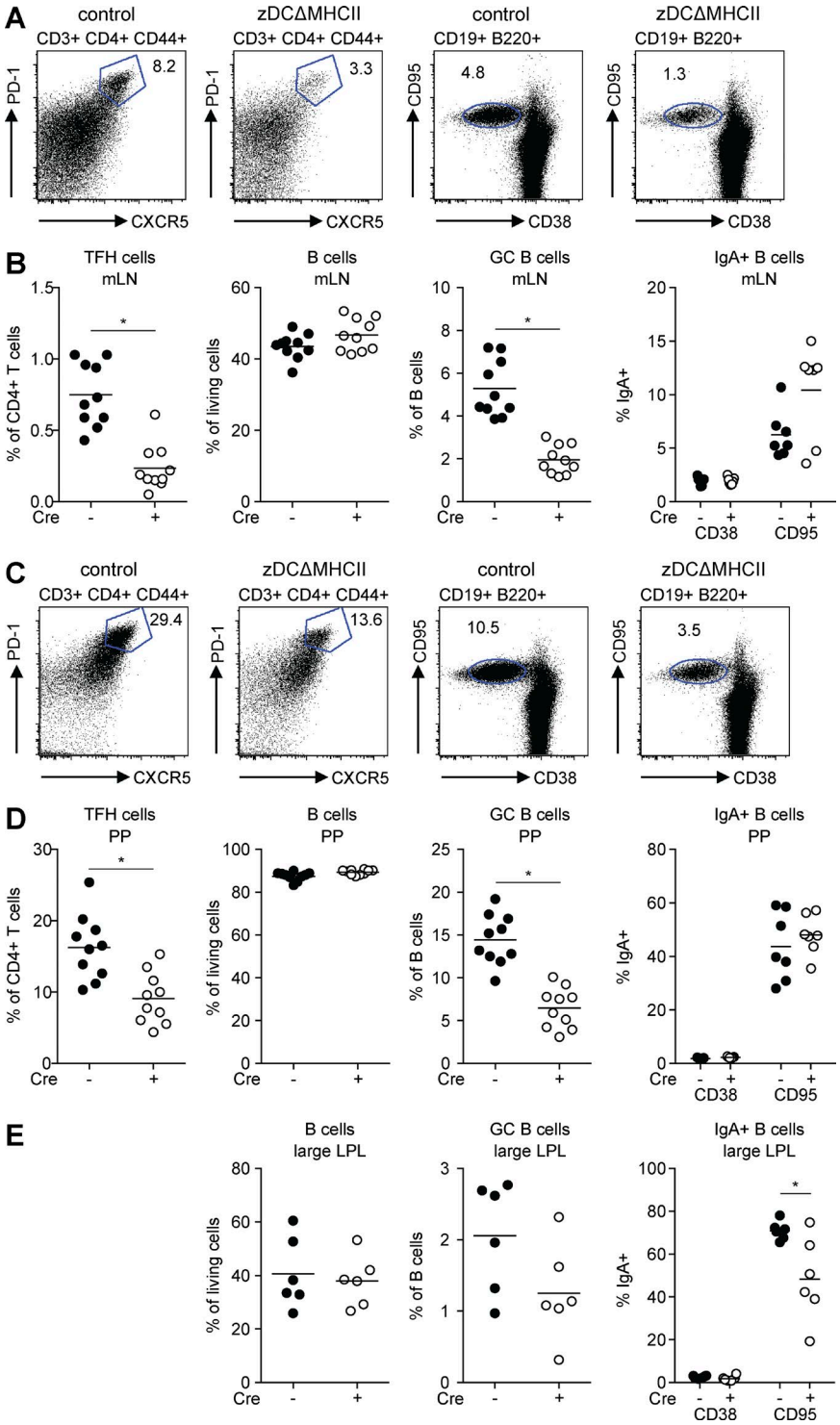

Figure 9. **Adaptive immune response against intestinal bacteria.** (A and C) Flow cytometric analysis of TFH cells ($CD3^+CD4^+CD62L^-CD44^+PD\text{-}1^+CXCR5^+$) and GC B cells ($CD19^+B220^+CD38^-CD95^+$) isolated from mLNs (A) and PPs (C) of control and zDCΔMHCII mice. (B and D) Graphs depict percentage of TFH cells among $CD4^+$ T cells, frequency of B cells among living cells, percentage of GC B cells among B cells, and frequency of IgA^+ B cells in mLNs (B) and PPs (D). Each data point represents one individual mouse ($n = 7–10$). (E) Graphs depict frequency of B cells among living cells, percentage of GC B cells among B cells, and frequency of IgA^+ B cells in the lamina propria of the large intestine ($n = 6$). *, $P < 0.05$.

was amplified and sequenced with the Illumina Miseq platform, as described previously (Buffie et al., 2015). Sequences were analyzed using version 1.33.3 of the MOTHUR pipeline (Schloss et al., 2009) as described in Buffie et al. (2015). Sequences with distance-based similarity of at least 97% were assigned the same OTU (operational taxonomic unit) and representative OTUs were classified using a modified Greengenes reference database (DeSantis et al., 2006).

Colonization of germ-free mice. Germ-free control and zDCΔMHCII mice were colonized with a mix of six in-

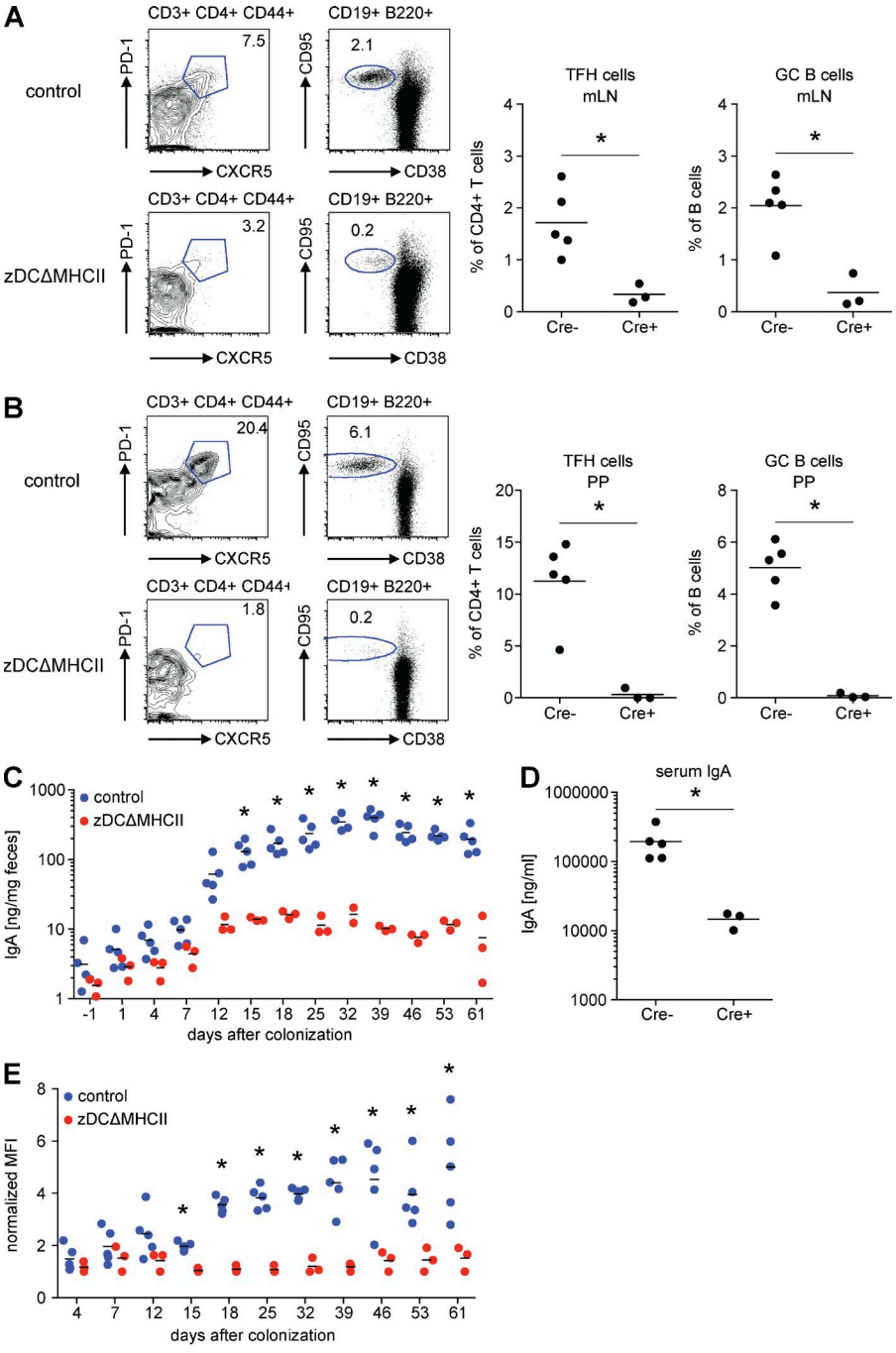

Figure 10. **Colonization of germ-free mice.** Germ-free control and zDCΔMHCII mice were colonized with a mixture of six different intestinal bacteria. Flow cytometric analysis of TFH cells ($CD3^+CD4^+CD62L^-CD44^+PD\text{-}1^+CXCR5^+$) and GC B cells ($CD19^+B220^+CD38^-CD95^+$) isolated from mLNs (A) and PPs (B) of control and zDCΔMHCII mice 61 d after colonization. Graphs depict percentage of TFH cells among $CD4^+$ T cells and percentage of GC B cells among all B cells in mLNs (A) and PPs (B). Each data point represents one individual mouse (n = 3–5). (C and D) Graphs depict amount of total IgA in feces (C) and serum (D) 61 d after colonization. Each data point represents one individual mouse (n = 3–5). (E) Bacteria were isolated from the feces of control and zDCΔMHCII mice and stained with anti-mouse-IgA. Graph depicts normalized MFI of IgA coated bacteria. Each data point represents one individual mouse (n = 3–5). *, $P < 0.05$.

testinal bacteria (*E. coli* [LF82], *E. faecalis*, *B. longum*, *L. plantarum*, *B. vulgatus*, and *R. gnavus*). Colonization was assessed by PCR using following primers: *E. faecalis* forward, 5′-CCCTTATTGTTAGTTGCCATCATT-3′ *E. faecalis* reverse,5′-ACTCGTTGTACTTCCCATTGT-3′;*B.longum* forward, 5′-GGGTGGTAATGCCGGATG-3′ *B. longum* reverse, 5′-TAAGCGATGGACTTTCACACC-3′; *L. plantarum* forward, 5′-AGCAGTAGGGAATCTTCCA-3′ *L. plantarum* reverse, 5′-CACCGCTACACATGGAG-3′; *B. vulgatus* forward, 5′-GGTGTCGGCTTAAGTGCCAT-3′ *B. vulgatus* reverse, 5′-CGGAYGTAAGGGCCGTGC-3′; *R. gnavus* forward, 5′-GGAGCAGACCAGATCCAA AT-3′ *R. gnavus* reverse, 5′-CCAATATACATTCCCGGT CTTT-3′; *E. coli* forward, 5′-CCATTCATGCAGCAG CTCTTT-3′ *E. coli* reverse, 5′-ATCGGACAACATTAG CGGTGT-3′. Coating of bacteria with endogenous IgA and amount of total IgA in the serum and feces was determined at indicated time points.

Statistical analysis. Results are shown as means + SEM. Comparisons between groups was done using Student's two-tailed *t* test analysis. Statistical significance was determined as p-values <0.05.

Online supplemental material. Fig. S1 shows flow cytometric analysis of $zDC^{Cre+}IRF4^{wt/fl}$ reporter mice. Fig. S2 show bacteria-specific PCR to confirm colonization of germ-free mice. Online supplemental material is available at http://www.jem.org/cgi/content/full/jem.20160062/DC1.

ACKNOWLEDGMENTS

We are grateful to members of the Nussenzweig laboratory for helpful discussion, reagents, and critical reading of the manuscript.

This work was supported in part by National Institutes of Health grant number AI 13013. M.C. Nussenzweig is a Howard Hughes Medical Institute investigator.

The authors declare no competing financial interests.

Submitted: 13 January 2016
Accepted: 12 February 2016

REFERENCES

Basu, R., D.B. O'Quinn, D.J. Silberger, T.R. Schoeb, L. Fouser, W. Ouyang, R.D. Hatton, and C.T. Weaver. 2012. Th22 cells are an important source of IL-22 for host protection against enteropathogenic bacteria. *Immunity.* 37:1061–1075. http://dx.doi.org/10.1016/j.immuni.2012.08.024

Bernink, J.H., L. Krabbendam, K. Germar, E. de Jong, K. Gronke, M. Kofoed-Nielsen, J.M. Munneke, M.D. Hazenberg, J. Villaudy, C.J. Buskens, et al. 2015. Interleukin-12 and -23 control plasticity of $CD127^+$ group 1 and group 3 innate lymphoid cells in the intestinal lamina propria. *Immunity.* 43:146–160. http://dx.doi.org/10.1016/j.immuni.2015.06.019

Birnberg, T., L. Bar-On, A. Sapoznikov, M.L. Caton, L. Cervantes-Barragán, D. Makia, R. Krauthgamer, O. Brenner, B. Ludewig, D. Brockschnieder, et al. 2008. Lack of conventional dendritic cells is compatible with normal development and T cell homeostasis, but causes myeloid proliferative syndrome. *Immunity.* 29:986–997. http://dx.doi.org/10.1016/j.immuni.2008.10.012

Bogunovic, M., F. Ginhoux, J. Helft, L. Shang, D. Hashimoto, M. Greter, K. Liu, C. Jakubzick, M.A. Ingersoll, M. Leboeuf, et al. 2009. Origin of the lamina propria dendritic cell network. *Immunity.* 31:513–525. http://dx.doi.org/10.1016/j.immuni.2009.08.010

Brenchley, J.M., D.A. Price, T.W. Schacker, T.E. Asher, G. Silvestri, S. Rao, Z. Kazzaz, E. Bornstein, O. Lambotte, D. Altmann, et al. 2006. Microbial translocation is a cause of systemic immune activation in chronic HIV infection. *Nat. Med.* 12:1365–1371. http://dx.doi.org/10.1038/nm1511

Buffie, C.G., V. Bucci, R.R. Stein, P.T. McKenney, L. Ling, A. Gobourne, D. No, H. Liu, M. Kinnebrew, A. Viale, et al. 2015. Precision microbiome reconstitution restores bile acid mediated resistance to *Clostridium difficile*. *Nature.* 517:205–208. http://dx.doi.org/10.1038/nature13828

Caballero, S., and E.G. Pamer. 2015. Microbiota-mediated inflammation and antimicrobial defense in the intestine. *Annu. Rev. Immunol.* 33:227–256. http://dx.doi.org/10.1146/annurev-immunol-032713-120238

Caton, M.L., M.R. Smith-Raska, and B. Reizis. 2007. Notch-RBP-J signaling controls the homeostasis of $CD8^-$ dendritic cells in the spleen. *J. Exp. Med.* 204:1653–1664. http://dx.doi.org/10.1084/jem.20062648

Chassaing, B., G. Srinivasan, M.A. Delgado, A.N. Young, A.T. Gewirtz, and M.Vijay-Kumar. 2012. Fecal lipocalin 2, a sensitive and broadly dynamic non-invasive biomarker for intestinal inflammation. *PLoS One.* 7:e44328. http://dx.doi.org/10.1371/journal.pone.0044328

Chieppa, M., M. Rescigno, A.Y. Huang, and R.N. Germain. 2006. Dynamic imaging of dendritic cell extension into the small bowel lumen in response to epithelial cell TLR engagement. *J. Exp. Med.* 203:2841–2852. http://dx.doi.org/10.1084/jem.20061884

Crotty, S. 2011. Follicular helper CD4 T cells (TFH). *Annu. Rev. Immunol.* 29:621–663. http://dx.doi.org/10.1146/annurev-immunol-031210-101400

Curtis, M.M., and S.S. Way. 2009. Interleukin-17 in host defence against bacterial, mycobacterial and fungal pathogens. *Immunology.* 126:177–185. http://dx.doi.org/10.1111/j.1365-2567.2008.03017.x

Darrasse-Jèze, G., S. Deroubaix, H. Mouquet, G.D. Victora, T. Eisenreich, K.H. Yao, R.F. Masilamani, M.L. Dustin, A. Rudensky, K. Liu, and M.C. Nussenzweig. 2009. Feedback control of regulatory T cell homeostasis by dendritic cells in vivo. *J. Exp. Med.* 206:1853–1862. http://dx.doi.org/10.1084/jem.20090746

DeSantis, T.Z., P. Hugenholtz, N. Larsen, M. Rojas, E.L. Brodie, K. Keller, T. Huber, D. Dalevi, P. Hu, and G.L. Andersen. 2006. Greengenes, a chimera-checked 16S rRNA gene database and workbench compatible with ARB. *Appl. Environ. Microbiol.* 72:5069–5072. http://dx.doi.org/10.1128/AEM.03006-05

Elinav, E., T. Strowig, A.L. Kau, J. Henao-Mejia, C.A. Thaiss, C.J. Booth, D.R. Peaper, J. Bertin, S.C. Eisenbarth, J.I. Gordon, and R.A. Flavell. 2011. NLRP6 inflammasome regulates colonic microbial ecology and risk for colitis. *Cell.* 145:745–757. http://dx.doi.org/10.1016/j.cell.2011.04.022

Gallo, R.L., and L.V. Hooper. 2012. Epithelial antimicrobial defence of the skin and intestine. *Nat. Rev. Immunol.* 12:503–516. http://dx.doi.org/10.1038/nri3228

Grajales-Reyes, G.E., A. Iwata, J. Albring, X. Wu, R. Tussiwand, W. Kc, N.M. Kretzer, C.G. Briseño, V. Durai, P. Bagadia, et al. 2015. Batf3 maintains autoactivation of Irf8 for commitment of a $CD8\alpha^+$ conventional DC clonogenic progenitor. *Nat. Immunol.* 16:708–717. http://dx.doi.org/10.1038/ni.3197

Hashimoto, K., S.K. Joshi, and P.A. Koni. 2002. A conditional null allele of the major histocompatibility IA-beta chain gene. *Genesis.* 32:152–153. http://dx.doi.org/10.1002/gene.10056

Hildner, K., B.T. Edelson, W.E. Purtha, M. Diamond, H. Matsushita, M. Kohyama, B. Calderon, B.U. Schraml, E.R. Unanue, M.S. Diamond, et al. 2008. Batf3 deficiency reveals a critical role for $CD8alpha^+$ dendritic cells in cytotoxic T cell immunity. *Science.* 322:1097–1100. http://dx.doi.org/10.1126/science.1164206

Hohl, T.M., A. Rivera, L. Lipuma, A. Gallegos, C. Shi, M. Mack, and E.G. Pamer. 2009. Inflammatory monocytes facilitate adaptive CD4 T cell responses during respiratory fungal infection. *Cell Host Microbe.* 6:470–481. http://dx.doi.org/10.1016/j.chom.2009.10.007

Ivanov, I.I., K. Atarashi, N. Manel, E.L. Brodie, T. Shima, U. Karaoz, D. Wei, K.C. Goldfarb, C.A. Santee, S.V. Lynch, et al. 2009. Induction of intestinal Th17 cells by segmented filamentous bacteria. *Cell.* 139:485–498. http://dx.doi.org/10.1016/j.cell.2009.09.033

Johansen, F.E., M. Pekna, I.N. Norderhaug, B. Haneberg, M.A. Hietala, P. Krajci, C. Betsholtz, and P. Brandtzaeg. 1999. Absence of epithelial immunoglobulin A transport, with increased mucosal leakiness, in polymeric immunoglobulin receptor/secretory component-deficient mice. *J. Exp. Med.* 190:915–922. http://dx.doi.org/10.1084/jem.190.7.915

Jung, S., D. Unutmaz, P. Wong, G. Sano, K. De los Santos, T. Sparwasser, S. Wu, S. Vuthoori, K. Ko, F. Zavala, et al.. 2002. In vivo depletion of $CD11c^+$ dendritic cells abrogates priming of $CD8^+$ T cells by exogenous cell-associated antigens. *Immunity.* 17:211–220. http://dx.doi.org/10.1016/S1074-7613(02)00365-5

Kassim, S.H., N.K. Rajasagi, X. Zhao, R. Chervenak, and S.R. Jennings. 2006. In vivo ablation of CD11c-positive dendritic cells increases susceptibility to herpes simplex virus type 1 infection and diminishes NK and T-cell responses. *J. Virol.* 80:3985–3993. http://dx.doi.org/10.1128/JVI.80.8.3985-3993.2006

Kato, L.M., S. Kawamoto, M. Maruya, and S. Fagarasan. 2014. Gut TFH and IgA: key players for regulation of bacterial communities and immune

homeostasis. *Immunol. Cell Biol.* 92:49–56. http://dx.doi.org/10.1038/icb.2013.54

Kinnebrew, M.A., C.G. Buffie, G.E. Diehl, L.A. Zenewicz, I. Leiner, T.M. Hohl, R.A. Flavell, D.R. Littman, and E.G. Pamer. 2012. Interleukin 23 production by intestinal $CD103^+CD11b^+$ dendritic cells in response to bacterial flagellin enhances mucosal innate immune defense. *Immunity.* 36:276–287. http://dx.doi.org/10.1016/j.immuni.2011.12.011

Klein, U., S. Casola, G. Cattoretti, Q. Shen, M. Lia, T. Mo, T. Ludwig, K. Rajewsky, and R. Dalla-Favera. 2006. Transcription factor IRF4 controls plasma cell differentiation and class-switch recombination. *Nat. Immunol.* 7:773–782. http://dx.doi.org/10.1038/ni1357

Kubinak, J.L., C. Petersen, W.Z. Stephens, R. Soto, E. Bake, R.M. O'Connell, and J.L. Round. 2015. MyD88 signaling in T cells directs IgA-mediated control of the microbiota to promote health. *Cell Host Microbe.* 17:153–163. http://dx.doi.org/10.1016/j.chom.2014.12.009

Lewis, K.L., M.L. Caton, M. Bogunovic, M. Greter, L.T. Grajkowska, D. Ng, A. Klinakis, I.F. Charo, S. Jung, J.L. Gommerman, et al. 2011. Notch2 receptor signaling controls functional differentiation of dendritic cells in the spleen and intestine. *Immunity.* 35:780–791. http://dx.doi.org/10.1016/j.immuni.2011.08.013

Lindquist, R.L., G. Shakhar, D. Dudziak, H. Wardemann, T. Eisenreich, M.L. Dustin, and M.C. Nussenzweig. 2004. Visualizing dendritic cell networks in vivo. *Nat. Immunol.* 5:1243–1250. http://dx.doi.org/10.1038/ni1139

Macpherson, A.J., and T. Uhr. 2004. Induction of protective IgA by intestinal dendritic cells carrying commensal bacteria. *Science.* 303:1662–1665. http://dx.doi.org/10.1126/science.1091334

Mangan, P.R., L.E. Harrington, D.B. O'Quinn, W.S. Helms, D.C. Bullard, C.O. Elson, R.D. Hatton, S.M. Wahl, T.R. Schoeb, and C.T. Weaver. 2006. Transforming growth factor-β induces development of the T_H17 lineage. *Nature.* 441:231–234. http://dx.doi.org/10.1038/nature04754

Maruya, M., S. Kawamoto, L.M. Kato, and S. Fagarasan. 2013. Impaired selection of IgA and intestinal dysbiosis associated with PD-1-deficiency. *Gut Microbes.* 4:165–171. http://dx.doi.org/10.4161/gmic.23595

Meredith, M.M., K. Liu, G. Darrasse-Jeze, A.O. Kamphorst, H.A. Schreiber, P. Guermonprez, J. Idoyaga, C. Cheong, K.H. Yao, R.E. Niec, and M.C. Nussenzweig. 2012. Expression of the zinc finger transcription factor zDC (Zbtb46, Btbd4) defines the classical dendritic cell lineage. *J. Exp. Med.* 209:1153–1165. http://dx.doi.org/10.1084/jem.20112675

Niess, J.H., S. Brand, X. Gu, L. Landsman, S. Jung, B.A. McCormick, J.M. Vyas, M. Boes, H.L. Ploegh, J.G. Fox, et al. 2005. CX3CR1-mediated dendritic cell access to the intestinal lumen and bacterial clearance. *Science.* 307:254–258. http://dx.doi.org/10.1126/science.1102901

Nussenzweig, M.C., R.M. Steinman, B. Gutchinov, and Z.A. Cohn. 1980. Dendritic cells are accessory cells for the development of anti-trinitrophenyl cytotoxic T lymphocytes. *J. Exp. Med.* 152:1070–1084. http://dx.doi.org/10.1084/jem.152.4.1070

Ohnmacht, C., A. Pullner, S.B. King, I. Drexler, S. Meier, T. Brocker, and D. Voehringer. 2009. Constitutive ablation of dendritic cells breaks self-tolerance of CD4 T cells and results in spontaneous fatal autoimmunity. *J. Exp. Med.* 206:549–559. http://dx.doi.org/10.1084/jem.20082394

Palm, N.W., M.R. de Zoete, T.W. Cullen, N.A. Barry, J. Stefanowski, L. Hao, P.H. Degnan, J. Hu, I. Peter, W. Zhang, et al. 2014. Immunoglobulin A coating identifies colitogenic bacteria in inflammatory bowel disease. *Cell.* 158:1000–1010. http://dx.doi.org/10.1016/j.cell.2014.08.006

Park, S.G., R. Mathur, M. Long, N. Hosh, L. Hao, M.S. Hayden, and S. Ghosh. 2010. T regulatory cells maintain intestinal homeostasis by suppressing γδ T cells. *Immunity.* 33:791–803. http://dx.doi.org/10.1016/j.immuni.2010.10.014

Perry, J.S., C.W. Lio, A.L. Kau, K. Nutsch, Z. Yang, J.I. Gordon, K.M. Murphy, and C.S. Hsieh. 2014. Distinct contributions of Aire and antigen-presenting-cell subsets to the generation of self-tolerance in the thymus. *Immunity.* 41:414–426. http://dx.doi.org/10.1016/j.immuni.2014.08.007

Persson, E.K., H. Uronen-Hansson, M. Semmrich, A. Rivollier, K. Hägerbrand, J. Marsal, S. Gudjonsson, U. Håkansson, B. Reizis, K. Kotarsky, and W.W. Agace. 2013. IRF4 transcription-factor-dependent $CD103^+CD11b^+$ dendritic cells drive mucosal T helper 17 cell differentiation. *Immunity.* 38:958–969. http://dx.doi.org/10.1016/j.immuni.2013.03.009

Salzman, N.H., H. de Jong, Y. Paterson, H.J. Harmsen, G.W. Welling, and N.A. Bos. 2002. Analysis of 16S libraries of mouse gastrointestinal microflora reveals a large new group of mouse intestinal bacteria. *Microbiology.* 148:3651–3660. http://dx.doi.org/10.1099/00221287-148-11-3651

Sandler, N.G., and D.C. Douek. 2012. Microbial translocation in HIV infection: causes, consequences and treatment opportunities. *Nat. Rev. Microbiol.* 10:655–666. http://dx.doi.org/10.1038/nrmicro2848

Satpathy, A.T., W. Kc, J.C. Albring, B.T. Edelson, N.M. Kretzer, D. Bhattacharya, T.L. Murphy, and K.M. Murphy. 2012. Zbtb46 expression distinguishes classical dendritic cells and their committed progenitors from other immune lineages. *J. Exp. Med.* 209:1135–1152. http://dx.doi.org/10.1084/jem.20120030

Satpathy, A.T., C.G. Briseño, J.S. Lee, D. Ng, N.A. Manieri, W. Kc, X. Wu, S.R. Thomas, W.L. Lee, M. Turkoz, et al. 2013. Notch2-dependent classical dendritic cells orchestrate intestinal immunity to attaching-and-effacing bacterial pathogens. *Nat. Immunol.* 14:937–948. http://dx.doi.org/10.1038/ni.2679

Schlitzer, A., N. McGovern, P. Teo, T. Zelante, K. Atarashi, D. Low, A.W. Ho, P. See, A. Shin, P.S. Wasan, et al. 2013. IRF4 transcription factor-dependent $CD11b^+$ dendritic cells in human and mouse control mucosal IL-17 cytokine responses. *Immunity.* 38:970–983. http://dx.doi.org/10.1016/j.immuni.2013.04.011

Schloss, P.D., S.L. Westcott, T. Ryabin, J.R. Hall, M. Hartmann, E.B. Hollister, R.A. Lesniewski, B.B. Oakley, D.H. Parks, C.J. Robinson, et al. 2009. Introducing mothur: open-source, platform-independent, community-supported software for describing and comparing microbial communities. *Appl. Environ. Microbiol.* 75:7537–7541. http://dx.doi.org/10.1128/AEM.01541-09

Schreiber, H.A., J. Loschko, R.A. Karssemeijer, A. Escolano, M.M. Meredith, D. Mucida, P. Guermonprez, and M.C. Nussenzweig. 2013. Intestinal monocytes and macrophages are required for T cell polarization in response to Citrobacter rodentium. *J. Exp. Med.* 210:2025–2039. http://dx.doi.org/10.1084/jem.20130903

Serbina, N.V., T.P. Salazar-Mather, C.A. Biron, W.A. Kuziel, and E.G. Pamer. 2003. TNF/iNOS-producing dendritic cells mediate innate immune defense against bacterial infection. *Immunity.* 19:59–70. http://dx.doi.org/10.1016/S1074-7613(03)00171-7

Sonnenberg, G.F., L.A. Monticelli, M.M. Elloso, L.A. Fouser, and D. Artis. 2011. $CD4^+$ lymphoid tissue-inducer cells promote innate immunity in the gut. *Immunity.* 34:122–134. http://dx.doi.org/10.1016/j.immuni.2010.12.009

Steinman, R.M., D. Hawiger, and M.C. Nussenzweig. 2003. Tolerogenic dendritic cells. *Annu. Rev. Immunol.* 21:685–711. http://dx.doi.org/10.1146/annurev.immunol.21.120601.141040

Stranges, P.B., J. Watson, C.J. Cooper, C.M. Choisy-Rossi, A.C. Stonebraker, R.A. Beighton, H. Hartig, J.P. Sundberg, S. Servick, G. Kaufmann, et al. 2007. Elimination of antigen-presenting cells and autoreactive T cells by Fas contributes to prevention of autoimmunity. *Immunity.* 26:629–641. http://dx.doi.org/10.1016/j.immuni.2007.03.016

Swidsinski, A., J. Weber, V. Loening-Baucke, L.P. Hale, and H. Lochs. 2005. Spatial organization and composition of the mucosal flora in patients with inflammatory bowel disease. *J. Clin. Microbiol.* 43:3380–3389. http://dx.doi.org/10.1128/JCM.43.7.3380-3389.2005

Tamoutounour, S., S. Henri, H. Lelouard, B. de Bovis, C. de Haar, C.J. van der Woude, A.M. Woltman, Y. Reyal, D. Bonnet, D. Sichien, et al. 2012. CD64 distinguishes macrophages from dendritic cells in the gut and reveals the Th1-inducing role of mesenteric lymph node macrophages

during colitis. *Eur. J. Immunol.* 42:3150–3166. http://dx.doi.org/10.1002/eji.201242847

Tamura, T., P. Tailor, K. Yamaoka, H.J. Kong, H. Tsujimura, J.J. O'Shea, H. Singh, and K. Ozato. 2005. IFN regulatory factor-4 and -8 govern dendritic cell subset development and their functional diversity. *J. Immunol.* 174:2573–2581. http://dx.doi.org/10.4049/jimmunol.174.5.2573

Ubeda, C., Y. Taur, R.R. Jenq, M.J. Equinda, T. Son, M. Samstein, A. Viale, N.D. Socci, M.R. van den Brink, M. Kamboj, and E.G. Pamer. 2010. Vancomycin-resistant *Enterococcus* domination of intestinal microbiota is enabled by antibiotic treatment in mice and precedes bloodstream invasion in humans. *J. Clin. Invest.* 120:4332–4341. http://dx.doi.org/10.1172/JCI43918

Vaishnava, S., M. Yamamoto, K.M. Severson, K.A. Ruhn, X. Yu, O. Koren, R. Ley, E.K. Wakeland, and L.V. Hooper. 2011. The antibacterial lectin RegIIIγ promotes the spatial segregation of microbiota and host in the intestine. *Science.* 334:255–258. http://dx.doi.org/10.1126/science.1209791

Vallon-Eberhard, A., L. Landsman, N. Yogev, B. Verrier, and S. Jung. 2006. Transepithelial pathogen uptake into the small intestinal lamina propria. *J. Immunol.* 176:2465–2469. http://dx.doi.org/10.4049/jimmunol.176.4.2465